Formation of Donor-induced Quantum Dots in Si Nano-channels Observed by Kelvin Probe Force Microscope

THESIS

Formation of Donor-induced Quantum Dots in Si Nano-channels Observed by Kelvin Probe Force Microscope

TYSZKA KRZYSZTOF

Department of Nanovision Technology
Graduate School of Science and Technology,
Educational Division, Shizuoka University

June 2015

Abstract

Over the years the size of the field-effect transistor (FET) has been the main factor to be addressed when considering performance of silicon electronic devices. Nowadays, silicon technology is approaching the limits where further downscaling of conventional transistors is significantly hindered due to the discrete nature of dopants. To reach beyond the scaling limits, the concept of individual dopant-atoms used as building blocks of a device was introduced, underlying the new branch of electronic devices, namely dopant-atom transistors. In the basic variation of dopant-atom transistors, individual donors or cluster of donors placed within the FET channel works as a Quantum Dot (QD) allowing single electron tunneling transport.

In this work, formation of donor-induced QD in Si nano-channels doped by classical thermal diffusion with phosphorus (P) is addressed. The surface potential landscapes due to random P-donor distributions in FET channel are directly observed by Kelvin Probe Force Microscope (KPFM). As a new approach, comparative study is conducted by analysis of single-electron tunneling transport and surface potential measured by KPFM. The KPFM results are interpreted by correlation with surface potential simulation using Thomas-Fermi approximation.

At first, after the introductory part, experimental details are discussed. This includes silicon-on-insulator field-effect-transistor (SOI-FET) fabrication and explanation of experimental methods. Most importantly, it is emphasized that specific KPFM setup allows observation of FETs under operation. This allows investigation of FET channels depleted of screening electrons by negative back-gate biases. In the main part of the work the focus is placed on analysis and characterization of donor-induced QDs in different concentration regimes. In the experiment, two types of SOI-FET, representative for low-concentration regime (below metal-insulator transition, MIT) and high-concentration regime (above MIT) are investigated by KPFM and electrical characterization.

In the first step of analysis, internal structure of donor-induced QD and the number of formed QDs in different doping regimes is addressed. The source-drain current vs. gate voltage (ID-VG) characteristics confirm single electron tunneling in low temperatures for both concentration regimes. The observed ID-VG features (together with Coulomb diamonds analysis) suggest that for low gate voltages transport is governed by only one dominant QD. This is further confirmed by the KPFM observation of depleted FET channels potentials, showing features due to individual donors (low-concentration regime) and donor clusters (high-concentration regime). The potential landscapes are dominated by single deepest potential well which is ascribed to dominant QD, regardless of doping concentration. The effect is suppressed for higher gate voltages. This result coincides also with simulation. Further analysis, by using Monte Carlo approach, show that statistically doping concentration affects primary the structure of dominant QD. At low concentrations, individual donors form most of QDs (i.e. “donor-atom” QDs). At high concentrations above metal-insulator transition, closely-placed donors form more complex QDs (i.e. “donor-cluster” QDs).

In the second step of analysis dispersion of dominant QD, its relation to macroscopic potential features, and influence on tunneling transport is discussed. The KPFM results correlated with simulation show that dominant QD position dispersion is related to macroscopic potential features arising from superimposed potentials of many donors. This macroscopic potential strongly depends on doping concentration and dimensions of doped area, when screening by electrons is low. In low-concentration regime the potential landscape is dominated by potential wells due to individual donors. In high-concentration regime the deepest-potential QD is formed at the bottom of macroscopic potential well. The correlation with ID-VG characteristics shows that at low gate voltages, tunneling appears sequentially via strongly dispersed donor-atom QDs (in low-concentration regime) or one localized donor-cluster QD (in high-concentration regime).

In summery, for the first time, an experimental correlation between single-electron tunneling characteristics and potential landscapes was used to investigate formation of donor-induced QD in different doping regimes. This study provides insights for designing optimized dopant-atom devices in which either single dopants or clusters of many dopants can be utilized as dominant QD.

Contents

List of Abbreviations

AFM	Atomic Force Microscope
CMOS	Complementary Metal-Oxide-Semiconductor
CPD	Contact Potential Difference
EB	Electron-Beam
FET	Field-Effect Transistor
ITRS	International Technology Roadmap for Semiconductors
KPFM	Kelvin Probe Force Microscope
MIT	Metal-Insulator Transition
MOS	Metal-Oxide-Semiconductor
SET	Single Electron Transistor
SOI	Silicon-On-Insulator
SPM	Scanning Probe Microscope
STM	Scanning Tunneling Microscope
QD	Quantum Dot

1 Introduction

1.1 Research background

The history of modern electronics can be best described by the "law" formulated by Gordon Moore in 1965 [1]. Moore noticed that the number of transistors than can fit on a silicon chip doubles every two years as technology advances. Not as a physical law but more as a prediction, he claimed that this trend will continue for next 10 years. The "Moore's law" held true with good accuracy for next 50 years. However, this exponential growth can not last forever, at least not on the basis of conventional semiconductor technology. To let the downscaling trend persist new technologies are emerging, which will surely lead to further development. As Moore put it: "We've just seen the beginning of what computers are going to do for us" [2]

1.1.1 Dopant-atom transistors - to reach beyond the limits

Over the years the size of the Field-Effect Transistor (FET) was the main factor to be addressed while considering enhancement in performance of silicon based electronic devices. Following the Moore's law number of transistors per chip was exponentially increasing resulting in single transistor shrinking from dimensions of ~10µm to tens of nanometers at present [as shown in Fig.1-1(a)]. According to International Technology Roadmap for Semiconductors (ITRS 2013) [3] by the year 2015, the technology node of "10 nm" is the next target to be achieved. This means that single FET will reach sub-20nm scale. Considering such nano-dimensions the distribution of impurities in an FET channel can no longer be assumed uniform and discrete nature of dopants has to be taken into account [as shown in Fig.1-1(b)]. Many reports have already addressed this issue showing that random position and countable number of dopants in the channel of an FET, both significantly influence the nano-transistor's threshold level and electrical characteristics, accounting for poor device-to-device reproducibility [4-9]. Therefore, it is expected that further

downscaling of conventional transistors will be significantly hindered due to random dopant fluctuations, and conventional silicon technology is approaching its limits.

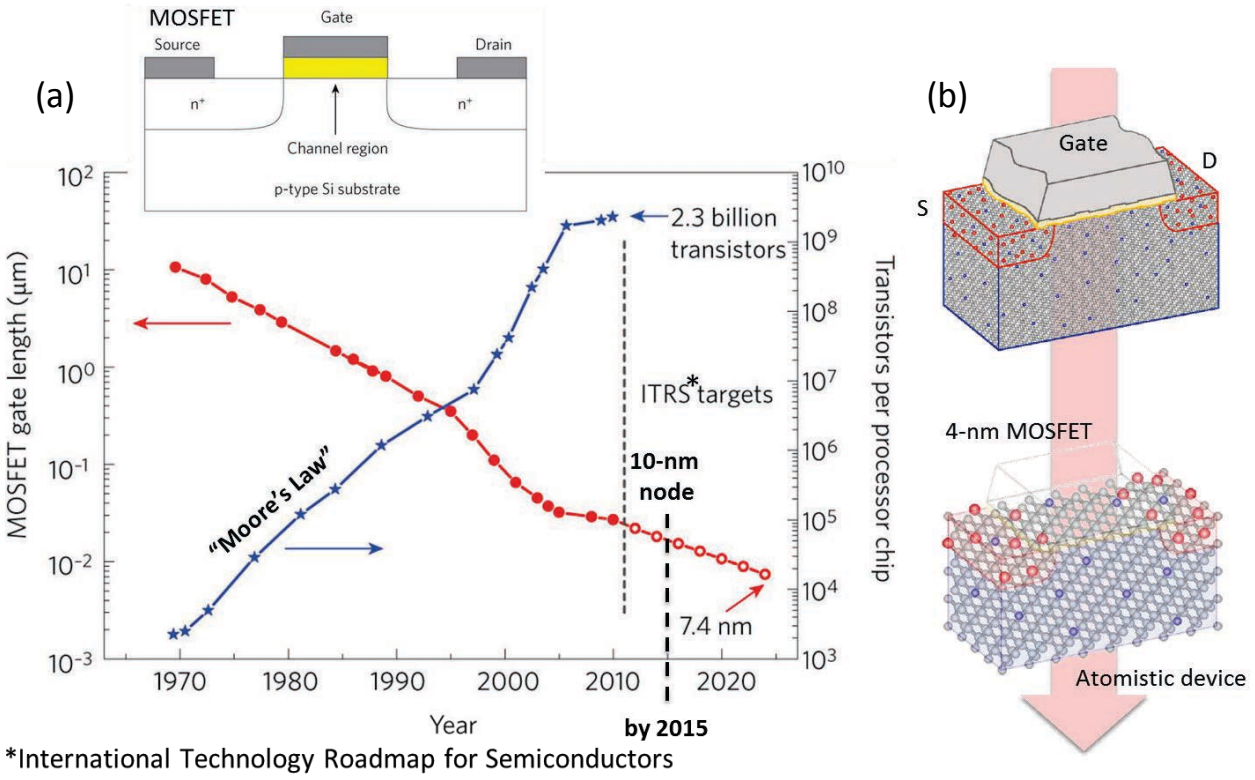

Fig. 4-6. (a) Illustration of Moor's law showing exponential change of number of transistors per chip over the years (blue line) and corresponding transistor gate length (red line). The 10-nm technology node is also marked as a target set by ITRS. Adapted from Ref. 10. (b) Schematic transformation of MOSFET from conventional device to atomistic "4-nm" device. Adapted from Ref.6

The need for new solutions led to the introduction of a concept of dopant-atoms used as building blocks of future devices, as a natural consequence of reaching the atomic scale. At the basis of this concept lays another preceding, extensively researched topic, so-called single-electron transistor (SET) allowing manipulation of electrons to the elementary level [11]. Such device consists of conductive nanometer-scale region ("island") placed between source (S) and drain (D) electrodes of a transistor, and gate electrode capacitively coupled to the island. In such structure the island is isolated form S and D by tunneling barriers and works as a Quantum Dot (QD) with discrete energy spectrum (if small enough). When properly tuned potential difference occurs between S and D, one electron can be

added to the island by tunneling through the barrier. The electron will occupy the lowest energy state and overall potential will be significantly raised, preventing other electrons from entering the island. The system will remain in this state until the overall potential is intentionally lowered by external gate bias application, allowing another electron to enter the island. This phenomenon is known as the Coulomb blockade effect [12], as the electron transfer is governed by Coulombic electrostatic repulsion between charges.

For Coulomb blockade to occur, several conditions have to be fulfilled regarding the SET structure. The island capacitance has to be small enough to prevent more than one electron to enter the island. The resistance of tunneling junction has to be tuned to meet same condition. In order to suppress thermally-activated tunneling events, the energy required to charge the island with one electron must be larger than thermal energy. The above conditions are directly related to the dimensions of an SET and impose the island size reduction. Typically, the single electron transport was studied at Low Temperatures (LT) which allowed loosening of the requirements regarding the island dimensions [13]. However, to allow room temperature (RT) operation, island's size has to be reduced to sub-10nm range [14]. Instead of problematic size reduction of Coulomb island, another approach is to use individual dopant atoms embedded in the semiconductor as an ultimate quantum dot allowing single electron tunneling. This regime lies at the basis of working principal of dopant-atom devices.

This work in particular refers to dopant-atom transistor as a basic building block of future nanoelectronic circuits. In the basic variation of dopant-atom transistor individual dopant or cluster of dopants placed within the FET channel works as a Quantum Dot (QD) allowing single electron tunneling transport.

The single electron transport via isolated impurities was initially observed as phenomenon for example in Ga-As based heterostructures [15, 16]. Transistor related research started with low temperature investigation of devices with dopant

atoms accidentally diffused into the channel of an FET [17-21]. In this case FET's nano-channel remains non-doped however due to side diffusion and channel's small length one or few individual dopants cross into it. The channel's potential can be modified by gate bias application. Therefore, if S and D are also biased and dopant related ground state is shifted and aligned with source Fermi level due to gate bias, single-electron tunneling transport can occur. This results in single current peak in LT I-V characteristic. The above studies provided a proof-of-concept for tunneling transport via isolated impurities in semiconductor underling the new branch of future electronic devices, namely dopant-atom devices. More complete description of such devices and single dopant approach can be found in Ref. 22 and 23.

As the advancing of methods of atomic manipulation continued, devices with dopant atoms intentionally placed in the channel became possible to realize. The sophisticated techniques such as single-ion-implantation [9, 24] or scanning tunneling microscope (STM) patterning [25], allowed controlled placement of one [24, 26-28] or few dopants [29, 30] and registration with electrostatic gates and readout devices. Although such processes represent the state-of-the-art in the field of dopant-atom nano-devices, they are far from industrial implementation. For example STM-based lithography requires removal of single atoms from hydrogen mask. Then, the system is treated with phosphine which bonds only with exposed Si. The removal of phosphine and hydrogen mask is followed by silicon overgrowth. This way controlled arrangements of P donors can be embedded into Si. This kind of process requires precise manipulation of H atoms which efficiency is limited by STM capabilities. Moreover, this and subsequent steps are time-consuming and have to be carried out in strictly controlled environment, drastically lowering the performance in comparison to conventional, Complementary Metal–Oxide–Semiconductor (CMOS) compatible processes.

To meet the demands of compatibility with today's semiconductor technology, the development of fabrication methods based on conventional processes is needed.

This demand was also addressed in Ref. 22 in words: "*Although the creation of artificial arrangements of impurities in a semiconductor by STM is rapidly approaching the level of atom manipulation on metal, no matter how exquisite this work might be it would be far more elegant if we could find self-assembly processes that arranged the impurities spontaneously.*"

Although state-of-the-art methods offer remarkable possibilities for studies, it is important to continue searching for simpler techniques. As an alternative, classical fabrication process, using low concentration random donor distribution was proposed in Ref.20. This study suggested possibility of statistically controlled formation of countable number of donor induced QD depending only on size of P-doped FET channel. This ultimately led to controlled fabrication of single P-atom based tunneling transistor operating in elevated temperatures [31]. Here the stub channel structure favored the single electron tunneling via single donor embedded in the channel. Recent studies also suggest possibility of controlled QD formation in nano-patterned transistor channels, using different doping regimes [32].

Thus, to clarify the possibility of controlled donor QD formation in naturally random donor distributions, further systematic study, including direct observation of donor arrangements is needed.

1.1.2 Dopant detection - Kelvin Probe Force Microscope (KPFM)

Nowadays the nanometrology techniques gain increasing importance mostly due to the semiconductor industry where troubleshooting and optimization of semiconductor devices requires knowledge about their electrical properties. Moreover, continuous development of new nanoscale electronic devices and materials places increasingly stringent demands on metrology [33]. The research often depends on proper measurement of dopant concentration and distribution which mainly determine the transport properties of semiconductor devices. However, direct observation of arrangements of dopants embedded in semiconductor structure requires development of new investigation methods with

accuracies in sub-10nm range, especially if considering metrology of dopant-atom devices described in previous section.

There are many classical methods which allow characterization of semiconductor devices parameters (doping concentration, electron mobility, resistivity, contact resistance, deep level impurities, interface states, barrier height etc.) in various ways, by current-voltage (I-V) characterization, Four-Point Probe (4PP), Hall effect measurements, ellipsometry, photoluminescence measurements, Raman spectroscopy, magnetic resonance or secondary ion mass spectroscopy (SIMS). More detail description of tools used for semiconductor characterization can be found in Ref. 34 or Ref. 35. By these methods, however, it is either difficult or impossible to obtain reliable information about presence or position of individual dopants embedded in the semiconductor.

The way to certainly define individual dopant presence and position is direct observation with atomic resolution. In last 50 years many methods intended for direct surface investigation with atomic lateral resolution were developed. Among these techniques great majority are methods based on Scanning Probe Microscopy (SPM) [36], electron or ion beam techniques (e.g. scanning transmission electron microscopy [37]) or field ion techniques (e.g. 3D-Atom Probe [38]). Here, electron microcopy is not considered because such methods, due to electron trapping in the interface states [39] or gate oxide after exposure to electron beam, may cause damage or affect the transistor operation [40] (e.g. alter the threshold voltage). Also ion beam techniques are omitted as, in principal, damaging or destructive measurements.

One important step towards atomic scale imaging of material structure was invention by G. Binning and H. Rohrer known as Scanning Tunneling Microscope (STM) [41]. In STM the atomically sharp tip, usually tungsten, scans the specially prepared surface of the conductive sample. During lateral scanning line by line, the biasing of a tip and sample leads to tunneling current through the nanometer scale

gap (air or vacuum) between them. Measured tunneling current is dependent on the tip-sample distance. Therefore, keeping tip-sample distance constant by feedback control application allows detection of tunneling current.

However, STM observation was limited only to conductive materials. The variation of this method allowing investigation of metals, semiconductors, and insulators is Atomic Force Microscope (AFM) [42]. This concept was also proposed by inventors of STM initiating the rapid development of SPMs. The crucial difference between AFM and STM is that instead of measuring tunneling currents, AFM detects Van der Waals forces, either repulsive or attractive interaction between tip and sample. Such forces occur between any materials therefore result of measurement depends only on the type of material and surface condition. Although until now few modes of AFM have been developed, the basic mode used in first version of AFM was contact mode which working principal is based on detection of prevailing short-range repulsive forces and chemical binding forces. However, due to the tip-sample contact, strong interactions can possibly cause damage to the sample surface, and atomic resolution cannot be achieved in stable manner. Another breakthrough in SPM development came with an introduction of non-contact mode AFM [43] for which topography measurement (mapping) was based on detection of long range attractive electrostatic forces between oscillating cantilever tip and fixed sample. Using this method F.J. Giessibl succeeded in imaging of Si (111)-(7x7) with atomic resolution in ultra-high vacuum (UHV) and room temperature [44].

Since then, evolution of probe microscopes started, initiating a new branch of tools, now considered one of the basic tools of nanometrology. Many new AFM-based methods, exploiting different physical phenomena were developed (e.g. Scanning Capacitance Microscopy – SCM, Scanning Spreading Resistance Microscopy – SSRM, Electrostatic Force Microscopy – EFM, Scanning Microwave Microscopy - SMM) allowing measurements of different material properties. The method which appears very useful in context of dopant detection is Kelvin Probe Force Microscopy

(KPFM) which was first introduced by Nonnenmacher [45]. The KPFM combines non-contact AFM with macroscopic Kelvin probe technique developed in 1898 by Lord Kelvin [46] for measurements of surface potentials [47, 48]. In present KPFM the cantilever senses the electrostatic force which builds up between grounded tip and sample due to work function difference. This work can be nullified by tip-sample biasing with voltage equal to Contac Potential Difference (CPD). Because the work function of doped semiconductor depends on doping concentration it was possible to use KPFM to detect doping profiles in such materials. Although at first the lateral resolution was in range of micrometers [45, 49]. Until now high-resolution KPFM imaging was achieved allowing detection of atomic scale surface potential variation or charge distribution [50-58]. In case of phosphorus doped Si particularly, it was possible to detect potential induced by ionized donors embedded in Si channel of FET [55, 56], electron injection in such donor potentials [57], and deep level dopants in depletion region of 2D p-n junction [58].

These reports show that thanks to high sensitivity to long-range electrostatic forces KFPM allows detection of charges embedded deeper in host material, which is crucial in case of individual dopant detection. In this context also, KPFM technique shows advantage over STM which allows charge detection limited to only few first atomic layers (although with higher lateral resolution). Therefore, in principle, KPFM can be considered a suitable technique to measure the surface potential induced by P-donors embedded in Si nano-transistor channels, which is in scope of this work.

1.2 Purpose of this work

Taking into consideration the background of the research presented in previous section it is clear that further study on innovative electronic devices is needed to prolong the validity of Moore's law. New concept of dopant-atom devices provides a good solution to push the limits of further downscaling, although, due to the lack of simple realization methods this solution can not be implemented into

industrial processes. One way to overcome the limitations is to develop CMOS compatible fabrication procedure based on classical processes. This topic was initially researched suggesting limited statistical control over donor-induced QD formation by nano-channel patterning, i.e. changing shape or dimensions of channel itself or channel doped area. Although the method is promising, further investigation is needed to extend the level of control. In particular, direct observation of different donor arrangements in relation to channel dimensions, shape and doping concentration can give more insight into controlled formation of donor-induced QD.

Therefore, in this work, formation mechanism of donor-induced QDs in Si nano-transistor channel doped by classical thermal diffusion with phosphorus (P) is addressed. To follow the requirements for CMOS compatibility devices are fabricated using classical methods like: resist-based Electron-Beam (EB) lithography, thermal oxidation, etching and thermal diffusion from spin coated source. The surface potential landscapes due to random P-donor distributions in FET channel are directly observed by KPFM with setup specially designed for this purpose. For reliable results, the research is conducted using new comparative approach, i.e. study by analysis of single-electron tunneling transport in correlation with surface potential measured by KPFM. The KPFM results are interpreted by additional correlation with surface potential simulation.

For clarity, the purpose of each research step is discussed in more detail as follows. At first, preliminary observation of donors' arrangements in Si channel doped with different doping concentration are done to identify characteristic features.

In the second step of analysis, internal structure of donor-induced QD and the number of formed QDs in different doping regimes are addressed. In particular, from this point work is focused on two types of devices, i.e. FET with lightly P-doped channel, and FET with selectively doped channel with high concentration of P. The

source-drain current vs. gate voltage (I_D-V_G) characteristics in correlation with KPFM observation and surface potential simulation are used to confirm single electron tunneling in low temperatures for both low and high concentration regimes, and to investigate structure of conducting QD.

In the next step, KPFM observation correlated with surface potential simulation is used for analysis of dispersion and evolution of dominant QD in uniformly and selectively doped devices. This is done in order to reveal QD dispersion in relation to macroscopic potential features, and its influence on tunneling transport. For further confirmation electrical characteristics of smaller devices with similar features and classical top gate, are taken.

The general purpose of this study is to provide insights for designing optimized dopant-atom devices, fabricated by means of classical methods, in which either single dopants or clusters of many dopants can be utilized as dominant QD in controlled manner.

1.3 Outline

This thesis describes methods used for observation of donor-induced QDs formed in FET nano-channel in different doping regimes, results of this observation along with conclusions, and perspectives for future studies. The thesis is structured into 6 chapters as summarized below.

In **Chapter 1**, as an introduction to this work, dopant-atom devices concept is presented as a way to reach beyond the miniaturization limits of future electronic devices. Particularly, importance of study of QD formation in random dopant distributions is emphasized. For purpose of this investigation Kelvin probe force microscopy is introduced as a tool for direct donor observation.

In **Chapter 2,** techniques and methods used in this study are described, this includes: KPFM working principle and setup for dopant detection, fabrication process of Silicon-On-Insulator (SOI) FET with different parameters, theory and

algorithm of surface potential simulation based on Thomas-Fermi approximations. As a new approach, comparative study by correlation of I-V characteristics with KPFM and simulation results is also addressed.

In **Chapter 3**, results of observation of different donors' arrangements in different doping regimes together with related physics are described. This chapter summarizes also previous KPFM observations allowing comparison between results for different doping concentrations. Such comparative analysis of potential landscape features allow to distinguish different donor systems, particularly: individual donors in charged and neutralized states - in room temperature and low temperature, closely placed individual donors or coupled donors, clusters of many donors formed in high concentration distributions.

In **Chapter 4**, internal structure of donor-induced QD and the number of formed QDs in different doping regimes are addressed. The observed source-drain current vs. gate voltage (I_D-V_G) characteristics suggest that for low gate voltages transport is governed by only one dominant QD. The potential landscapes are dominated by single deepest potential well which is ascribed to dominant QD, regardless of doping concentration. Further analysis, by using Monte Carlo approach, show that statistically doping concentration affects primary the structure of dominant QD suggesting that this parameter can be statistically controlled.

In **Chapter 5**, analysis of dispersion of dominant QD, its relation to macroscopic potential features, and influence on tunneling transport is discussed. By correlation of KPFM results with simulation it is found that dominant QD position dispersion is related to macroscopic potential features arising from superimposed potentials of many donors. This macroscopic potential strongly depends on doping concentration and dimensions of doped area. If is found that this macroscopic potential can favor central position of QD when channel is selectively doped with high concentration suggesting that this parameter can be statistically controlled.

In **Chapter 6**, the results of conducted study are summarized and general

conclusions are presented including future perspectives and remaining issues to be overcome to achieve optimized designed for dopant-based transistor which meets the requirements of classical CMOS fabrication methods.

2 Characterization of dopant-devices – Experimental details

2.1 Introduction

This chapter describes techniques and methods used in this study to characterize dopant-based transistors. As a new approach, in this work, comparative study is conducted by correlation of surface potential measured by KPFM and single-electron tunneling transport electrical characteristics. The KPFM results are interpreted by correlation with surface potential simulation including free electron screening. This kind of approach allows reliable investigation of influence of FET doping profile and channel structure on formation of donor-induced QDs and resulting I-V characteristics.

At first KPFM working principle and setup for dopant detection are discussed, fallowed by description of fabrication process of Silicon-On-Insulator (SOI) FET with different parameters. Chapter ends with brief explanations of theory and algorithm of surface potential simulation.

2.2 KPFM setup and measurement

Originally the KPFM was proposed by M. Nonnenmacher [45] as Atomic Force Microscope (AFM) employing the principal of Kelvin probe. Therefore, KPFM allows also determination of surface topography. The KPFM is sensitive to point charges located deeper below the surface of the measured sample [55]. For our purpose (detecting ionized P-donors in a Si channel), we use a specially-designed KPFM technique that allows measurements in ultra-high vacuum while bias can be applied to the electrodes from outside circuitry as during ordinary device operation. The schematic illustration of KPFM setup is shown in Fig.2-1.

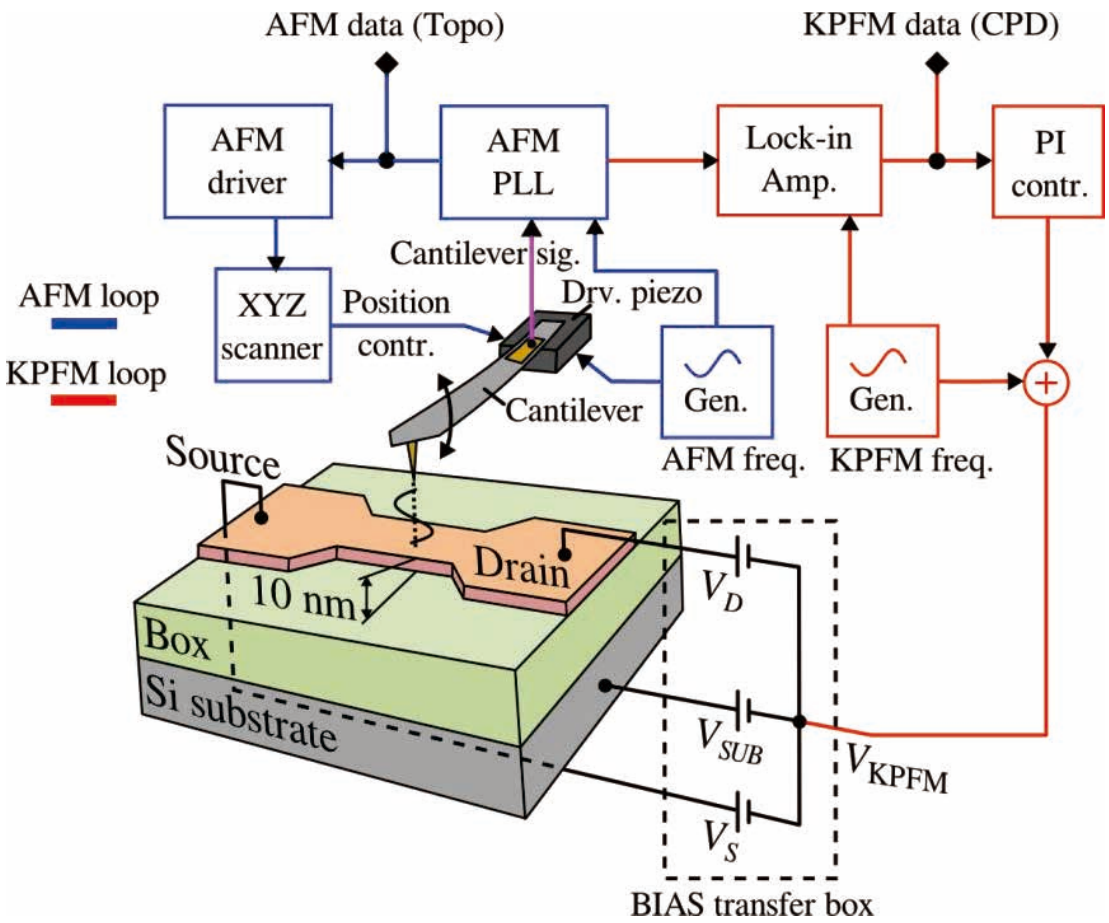

Fig. 2-1. The schematic illustration of KPFM setup and additional circuitry allowing depletion of FET channel (bias transfer box); FET structure is also schematically shown

The KPFM measurements are done in high vacuum (approx. 4×10^{-9} Torr) and room temperature (approx. 296 K). The working principle of KPFM is based on detection of long range electrostatic forces by the piezo-resistive cantilever tip scanning in proximity of the sample surface. The constant distance between the cantilever and the sample is maintained by AFM (AFM topography detection loop is marked blue in Fig.2-1). The cantilever oscillations are first excited by driving the piezo with specific AFM frequency matching the mechanical resonance frequency of a cantilever. In proximity of sample surface the attractive forces are acting on a cantilever. Due to the tip-sample interactions the cantilever bends and its resonant frequency is changing. This change is detected by Phase-Locked Loop (PLL) and recorded as a topography data. Simultaneously the “topo” signal is given as a feedback to AFM driver and cantilever’s Z position is readjusted to keep the same

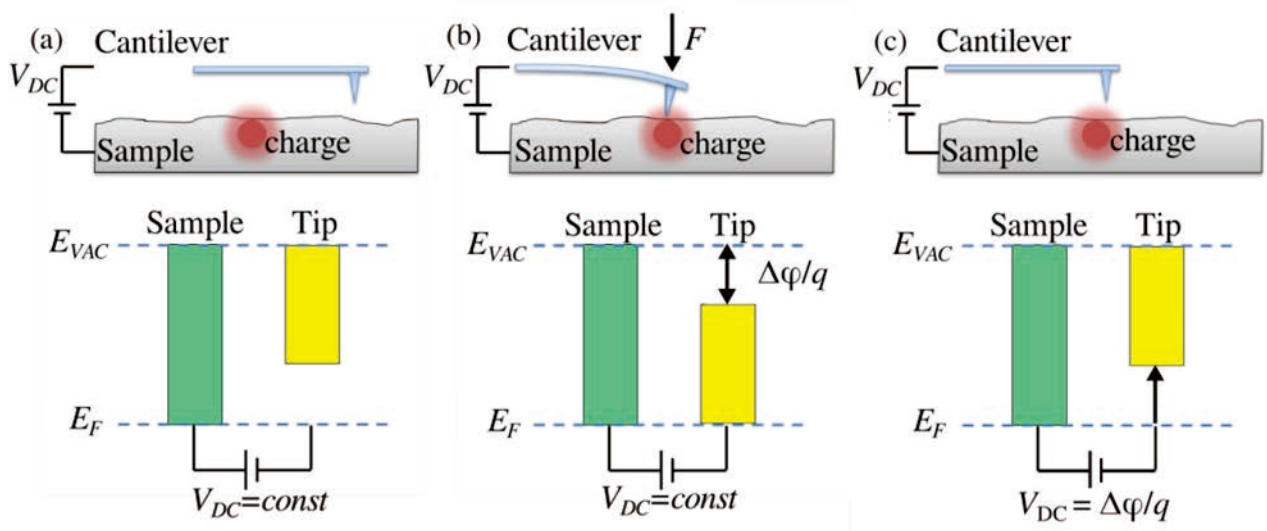

Fig.2-2 Schematic explanation of KPFM working principle; (a) System in equilibrium; (b) Electrostatic force (*F*) builds up; (c) Cancelation of *F* by V_{DS} bias application.

tip-sample distance. While the cantilever is scanning the surface in above manner it also detects the electrostatic forces which arise due to the work function difference between tip and sample, as shown in Fig.2-2. When the cantilever and the sample are in equilibrium, the V_{DC} is applied between them to compensate the initial work function difference between tip and sample [Fig.2-2(a)]. The attractive electrostatic force (*F*) builds up if some local change in work function occurs, as in Fig.2-2 (b). This force is cancelled by readjustment of V_{DC} which corresponds to a local Contact Potential Difference (CDP) as in Fig.2-2(c). To allow continuous detection of CPD, V_{DC} is modulated by specific KPFM bias frequency resulting in total tip-sample bias (V_{KPMF}). Electrostatic forces due to V_{KPMF} and local CPD cause deflection of cantilever which is detected first by AFM PLL, then directed to KPFM loop (marked red in Fig.2-1) and demodulated in Lock-in amplifier. This way KPFM data is obtained. The important difference between conventional KPFM setup and one presented here is the possibility of additional biasing of the sample (in this case the FET transistor), realized by bias transfer box (shown in Fig.2-1). For transistor V_{KPMF} works as a virtual ground. The FET is realized as a thin doped constriction (10 nm thick channels) between two wider pads of silicon - working as source (S) and drain (D) electrodes.

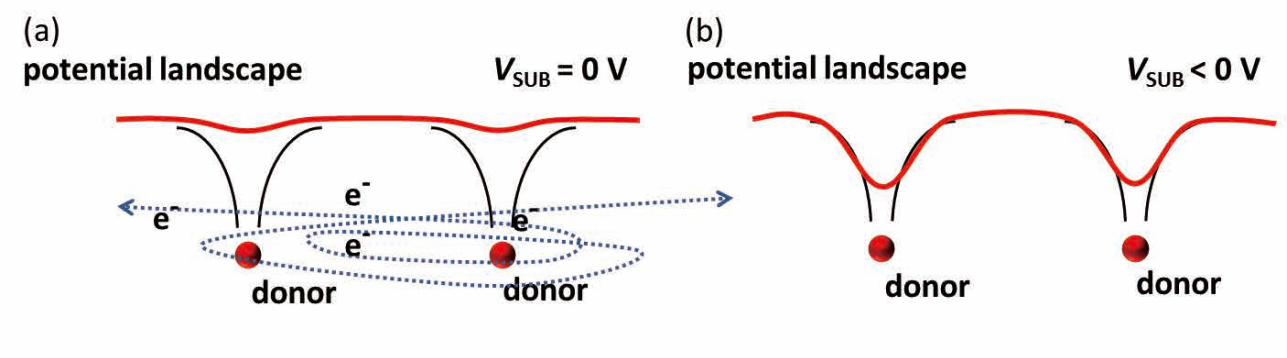

Fig.2-3. Influence of substrate bias application on measured potential landscape: (a) for channel screened by electrons, (b) for channel depleted of electrons.

The S/D electrodes are grounded (virtually) while the back gate bias (V_{SUB}) can be applied to the substrate (also in reference to V_{KPMF}). Such circuitry allows application of negative substrate bias to deplete free carriers (electrons) from the channel and thus, perform measurements of the surface potential dominantly induced by ionized P-donors [as shown in Fig.2-3]. By this method, it was possible to identify potential dips due to single donors and single acceptors [55, 56], successive electron charging in neighboring P-donors [57] and dopants with deeper energies in 2D *pn* junctions [58]. This previous experience confirms that the KPFM technique is suitable for observing dopant-induced potentials in thin Si channels under a variety of conditions.

The described KPMF setup is an invaluable nanometrology technique allowing detection of even individual dopants, investigation of electrical properties of FET by observation of donor-induced potential landscapes in thin nanoscale Si channels.

2.3 Fabrication of SOI-FET

Device fabrication is one of the important steps in this research work. For studying formation of donor-induced QDs in different doping regimes experimentally, we fabricated two types of silicon-on-insulator field-effect transistors (SOI-FETs) with thin channels (t_{Si}<10 nm) doped with P-donors. Fabrication was done with typical CMOS processing, by top Si patterning, using

thermal dry oxidation and etching processes. The channels are designed as nanoscale constrictions (patterned by an electron-beam lithography technique) formed between wider pads of Si (source and drain) as shown in Fig.2-4.

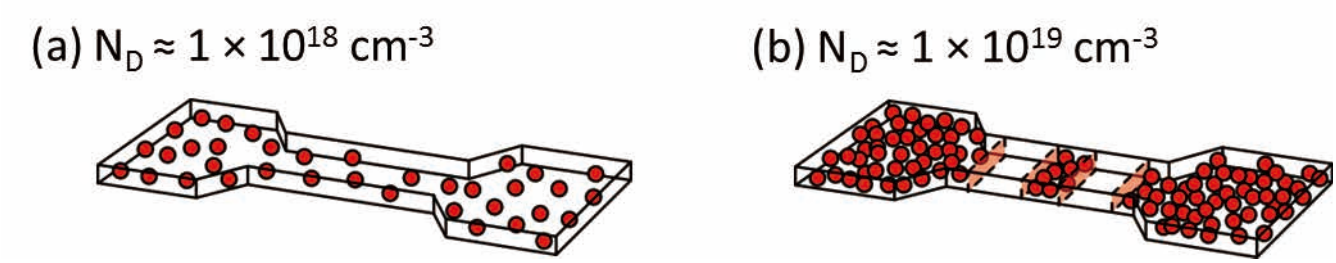

Fig.2-4. Schematic illustration of FET channel design: (a) for low concentration device, (b) for high concentration selectively doped device. Red dots are donors.

Doping of the channel with P-donors was done by thermal diffusion from a spin-coated silica film containing P_2O_3 at different concentrations, below and above the MIT point. Here, we focus on two types of devices, doped with $N_D \approx 1\times10^{18}$ cm^{-3} (low-concentration regime, below MIT) and, respectively, $N_D \approx 1\times10^{19}$ cm^{-3} (high-concentration regime, above MIT). For the high-concentration devices, the central highly-doped region was separated from the leads by non-doped gaps in order to allow more efficient depletion of carriers from the quasi-metallic region [as shown in Fig.2-4(b)]. The devices are differently designed for I-V measurements and KPFM

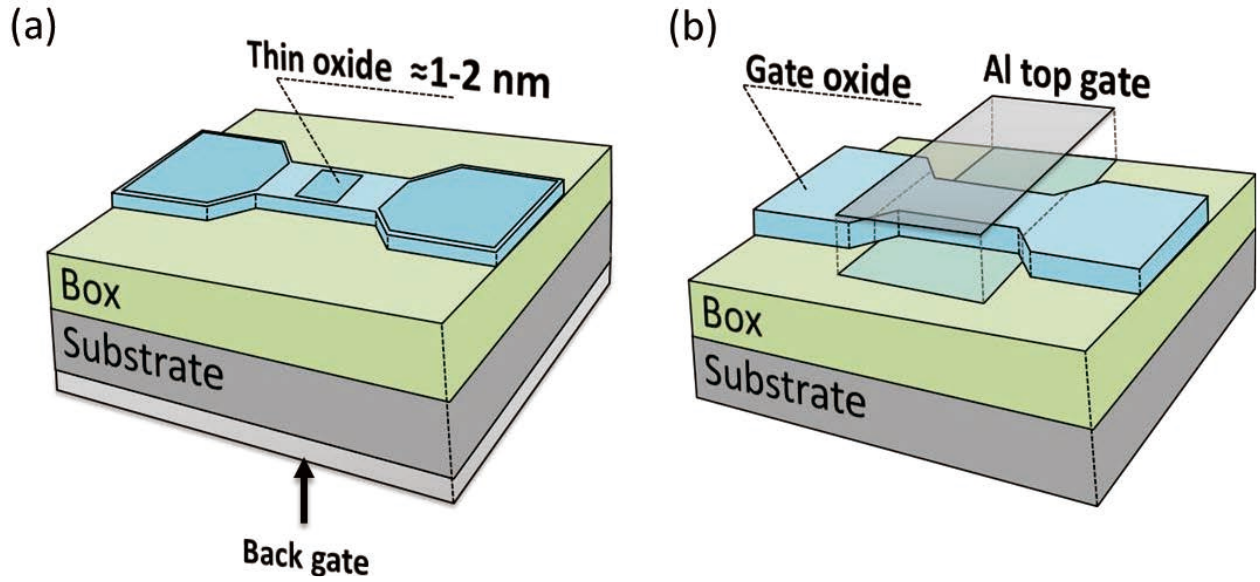

Fig.2-5. Schematic illustration of fabricated FETs: (a) for KPFM characterization, (b) for I-V characterization.

measurements. The main difference is the absence of a top gate for the KPFM devices in order to allow the KPFM tip to scan in proximity of the Si channel surface (through a 2-nm-thick thermally-grown SiO_2 layer) as shown in Fig.2-5(a). The ultrathin oxide layer works as a passivation film against unintentional contamination, while also allowing the cantilever to approach even closer to the Si top surface, thus giving the ability to observe dopants buried deeper in the Si channel. For I-V measurements, an Al top gate is used to control nanoscale channel potential, as shown in Fig. 2-5(b). Similarly, for KPFM devices, the same function is obtained by applying a negative bias to the *p*-type Si substrate (working as a backgate).

All fabrication steps which led to the final result, including thermal oxidation and doping were optimized. The full description of fabrication steps is contained in Appendix A. The systematic data obtained during optimization is presented in fabrication reports - Appendix B.

2.4 Surface potential simulation

In correlation with the KPFM measurements, we developed a simulation technique that allows evaluating the surface potential landscape induced by random distributions of P-donors in a thin (10 nm) Si layer with an adjustable scan area. Simulation setup is shown in Fig. 2-6. In this simulation, the bare potential is obtained by the superposition of Coulombic potential φ due to ionized P-donors calculated as:

$$\varphi(\boldsymbol{r}) = \frac{-e}{4\pi\epsilon_{Si}\boldsymbol{r}}$$

where ϵ_{Si} is dielectric constant for Si. This step is enough to simulate potentials induce by low concentration donor distributions in absence of electrons (unscreened). However, for high concentration donor distributions screening effect by free electrons has to be included [63, 64]. For this purpose, two-dimensional electron gas (2DEG) is introduced into the system. The electron density is calculated by solving self-consistently the 2D Thomas-Fermi equation and the Poisson equation

with periodic boundaries [65]. This calculation is based on Thomas –Fermi approximation [66,67] that local electron density n_e [m^{-2}] is proportional to the difference between chemical potential μ and local total potential φ_{tot}:

$$n_e = \frac{m_e e}{\pi\hbar^2}\left(\mu - \varphi_{tot}(n_e, \boldsymbol{r})\right),$$

where m_e is electron effective mass in Si. The screened potential is estimated at a height of 3 nm above the surface of Si (assuming 2-nm-thick SiO_2 layer and 1 nm tip-sample distance). The amount of screening electrons can be controlled by the electron coverage fraction (f_e) [63] in order to reproduce the effect of electron depletion induced by the gate voltage, as in the experiment.

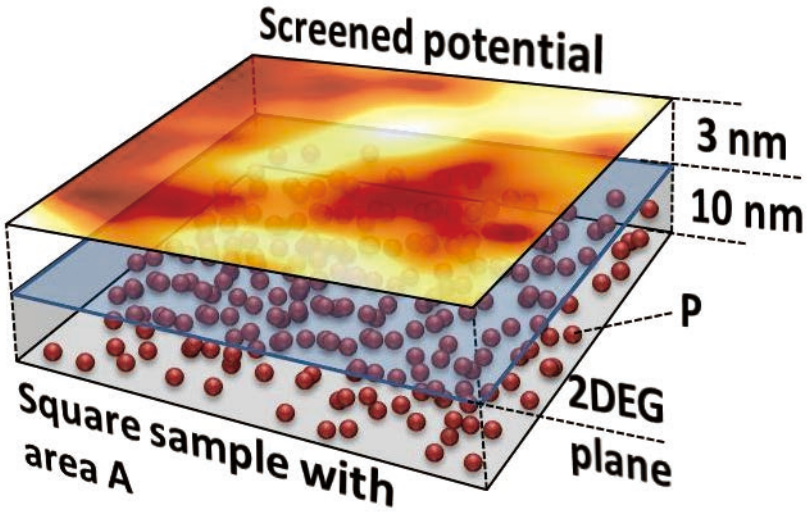

Fig.2-6. The schematic representation of surface potential simulation setup. Red dots correspond to individual donors placed randomly in 10-nm thick sheet with area A as a parameter. Two dimensional electron gas is placed on top of this sheet, while total surface potential is estimated at level of 3 nm from the surface.

3 Donors arrangement in different concentration regimes

This chapter is mainly based on:
K.Tyszka, D.Moraru, T.Mizuno, R.Jablonski and M.Tabe
Kelvin probe force microscope observation of donors' arrangement in Si transistor channel. Advanced Materials Research 1117:82-85 (2015).

3.1 Introduction

To date, a number of reports on dopant-based transistors have been published describing devices based on: solitary dopants which accidentally diffused into transistor channel [17-21]; individual dopants intentionally placed inside the channel by more complex fabrication techniques [24,26]; multiple-dopant QDs, fabricated by selective doping methods [31,32]. Measurements of I-V characteristics reveal drastic differences between devices with QDs containing different numbers of dopants [32]. To better understand this dependence, it is important to study possible dopants' arrangement as it directly influences the formation of QD in the channel. Therefore, we investigate configurations of dopants inside transistor channels doped with phosphorus at different concentrations (N_D). Proper interpretation of such KPFM observation of donors' arrangement in different doping regimes is crucial for this study, i.e. for purpose of correlation of single electron transport I-V characteristics via donor-induce QDs with measured donor induced potentials.

In this chapter, we summarize previous measurement results [55-57] obtained for devices doped with intermediate concentrations, and results, for heavily-doped devices, obtained particularly for investigation described in this thesis. We observed three basic configurations of dopants: solitary donors, neighboring donors, "clusters" of a few coupled donors, and "clusters" of many donors. This systematic observation provides information about the formation of quantum dots consisting of a single donor or a number of coupled donors.

3.2 KPFM measurement results

Our scanning probe system allows imaging of FET channel during operation, in temperatures ranging down to 13 K and in ultra-high vacuum. During all measurements, source and drain electrodes are biased in reference to KPFM bias (V_{KPFM}) and can be considered effectively grounded (for more details see s. 2.2). Different gate biases (V_{sub}) were applied to the substrate to achieve channel depletion. For all investigated devices the doping concentration was verified by 4-point probe measurement. For previously studied devices (in Ref.55-57), concentrations of $N_{D1} \approx 5\times10^{17}$ cm^{-3} and $N_{D2} \approx 1\times10^{18}$ cm^{-3} were used, and the channels were uniformly doped. The newly-fabricated FETs, with heavily-doped channels ($N_{D3} \geq 1\times10^{19}$ cm^{-3}), have the intentionally non-doped areas separating the doped part of the channel from the leads.

Devices doped with concentration N_{D1}.

Measurements were done at low temperature (LT) of 13 K, while applying V_{sub} = -3 V. By applying the bias, most of screening electrons are removed. In principle, in the absence of free carriers, the potential of all remaining fixed charges (donor ions) is superimposed, defining a resultant surface potential. However, at LT, most donors are neutral due to freeze-out effect. Only a small fraction of donors stays ionized inducing local potential fluctuations.

The KPFM images shown in Fig. 3-1 reveal uniformly-distributed potential dips [Fig. 3-1(a)] with circular shapes, suggesting point charges, such as solitary donors [Fig. 3-1(b)]. The diameter of the observed features varies from 5 nm to 10 nm, and matches the expected P-atom Bohr radius in Si ($a_{0P} \approx 2.5$ nm). The depth of the features (~25 mV) reflects potential well induced by P atoms buried deeper in silicon [55]. Expected potential for a P atom, close to channel surface, reaches ~45 mV and is decreasing for deeper-placed dopants due to the distance dependence of the Coulomb potential. Neighboring dips are distanced at ~10 to ~20 nm, which is also in

agreement with the average inter-donor distance $d_0 \approx 12$ nm for assumed N_{D1}.

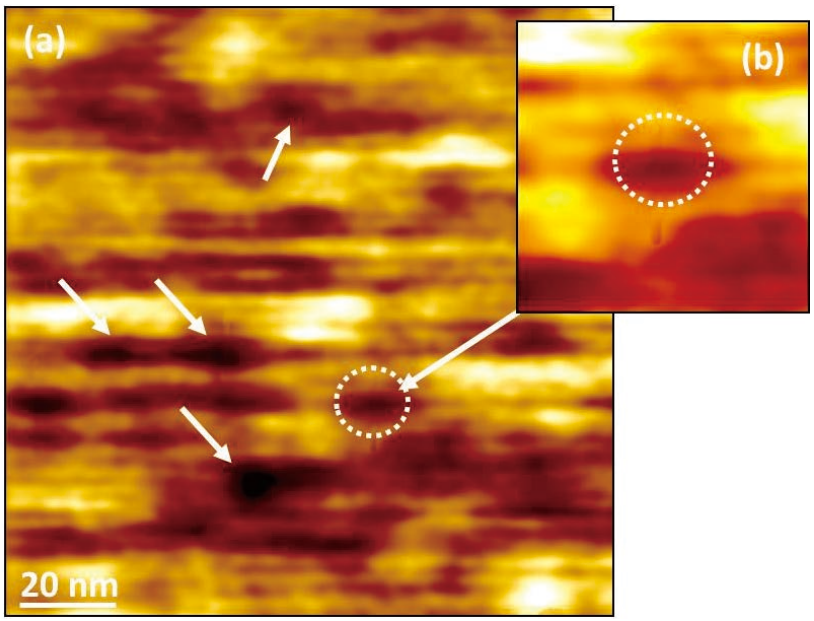

Fig.3-1. Potential landscape for $N_{D1} \approx 5\times10^{17}$ cm^{-3} measured under negative bias applied to the substrate. (a) Large-scale KPFM images. White arrows mark individual atoms. (b) Enlarged parts of (a) shows solitary donor marked with envelope. Adapted from Ref. 55

Devices doped with concentration N_{D2}.

For this case, KPFM images [Fig. 3-2] were obtained also in LT, under different V_{sub}, up to -3 V. We observed local surface potential modulation due to: (A) closely-placed solitary donors and (B) a few coupled donors [56]. In (A) case, slightly overlapping circular dips (~10 nm wide and 10-40 mV deep) are identified [Fig. 3-2(c)]. For (B) case, dark spots with irregular shapes, larger (in width and depth) than dips due to individual donors, are visible [Fig. 3-2(b)]. These deeper features can be ascribed to the superimposed potentials of a few (2 or 3) coupled donors, forming a multiple-donor "cluster". The above interpretation is in agreement with expected donor arrangement for N_{D2}. Average expected d is ~5.5 nm, which is about two times a_{0P}. Distinction between (A) and (B) cases was further confirmed by observation of potential profile dependence on applied V_{sub}, which is described later in this paper.

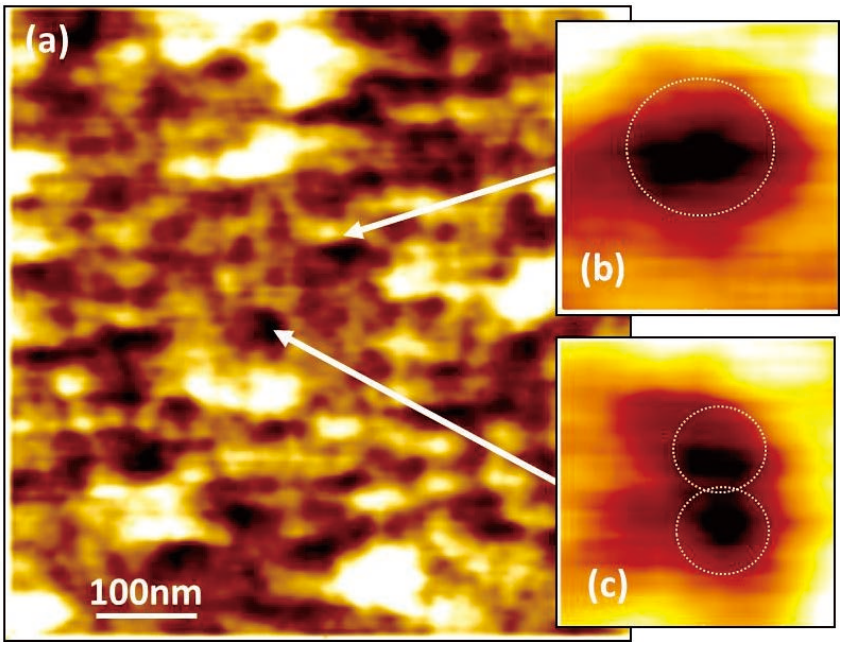

Fig.3-2. Potential landscape for $N_{D2} \approx 1\times10^{18}$ cm^{-3} measured under negative bias applied to the substrate. (a) Large-scale KPFM images. White arrows mark particular donor systems. (b) Enlarged parts of (a) show (c) closely-placed donors; (b) coupled donors. Adapted from Ref. 55

Devices doped with concentration N_{D3}.

For these devices, measurement was done at room temperature (RT), while V_{sub} was varied from 0 V to -4 V. The KPFM images reveal dark irregular dips [as shown in Fig. 3-3(a)], larger than for the systems of a few coupled donors presented above [Fig.3-2]. The depth of the potential in this area reaches ~150 mV, suggesting that potential well is induced by many closely-placed dopants. Considering that: (i) measurement was done in RT, (ii) there is no freeze-out effect, and (iii) N_{D2} is over critical concentration for Mott-transition [58]; we expect that bias is insufficient to fully deplete the channel. However, although donors are partially screened, fluctuations due to local concentration changes can still be observed. Since *d* varies from 4 to 2.5 nm in this sample, all donors are strongly interacting and solitary donors cannot be distinguished. The image contrast comes from two main effects: (a) superposition of potentials due to partially-ionized donors and (b) distribution of remaining screening electrons. The higher resolution image of middle part of slit

with enhanced contrast [Fig.3-3(b)] shows more detail structure. The darker areas in the image correspond most likely to higher local concentration of P donors, i.e. donor clusters [60]. The result suggests high non-uniformity of donor distribution even in such high concentration.

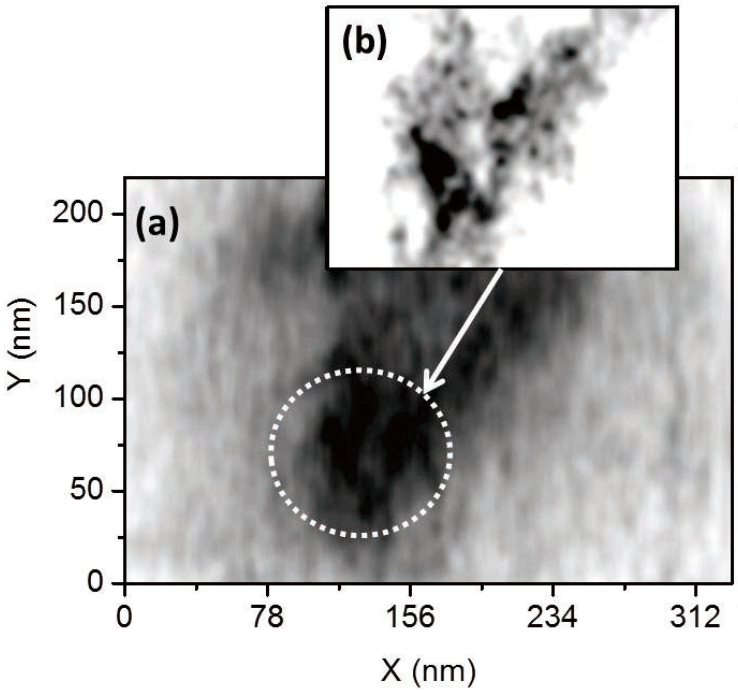

Fig.3-3. Potential landscape for N_{D3}≈1×10^{19}cm^{-3} measured under negative bias V_{sub} = -4V applied to the substrate. (a) Large-scale KPFM image shows potential of doped slit. Enlarged parts of (a) show (b) detail structure due to non-uniformly distributed donors. The irregular dark dips correspond to donor clusters.

3.3 Charging and discharging mechanism.

We also acquired images for gradually changing V_{sub} in LT and RT, in order to observe charging and discharging mechanism. For N_{D1}, LT results show local decrease of contrast (flattening of potential) while increasing V_{sub}. This is due to the injection of additional electrons into single donors. Moreover, by application of small source to drain bias, V_{DS} = 5 mV, we can even observe charging effects in transport via single donors [57].

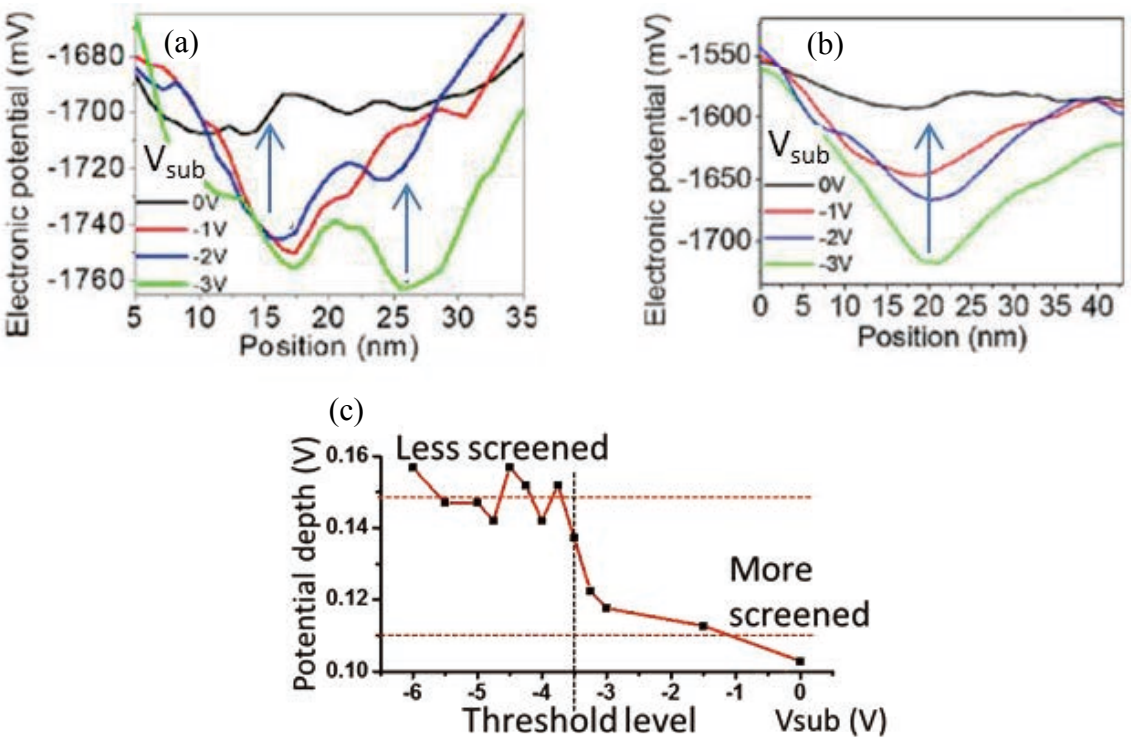

Fig. 3-4. Surface potential line profiles over: (a) two closely-placed donors, (b) few coupled donors [56]. Electron filling into donors is observed. Blue arrows indicate direction of potential depth change while V_{sub} changes from -3 V to 0 V. (c) Average potential depth dependence on V_{sub} for N_{D3}. Effect of screening electrons on the potential depth is observable.

For N_{D2}, electron filling was observed at LT for the two cases described earlier (A, B). For closely-placed donors, electron filling appears as full neutralization of each of the neighboring donors. When more negative bias is applied gradually, all donors are ionized one by one [as potential profiles shown in Fig. 3-4(a)]. For coupled donors, gradual electron removal appears as progressive lowering of the potential profile over the whole area of the donor "cluster" [as shown in Fig 3-4(b)]. This is natural as it is expected that electron wave function is spread over interacting donors and, thus, the donors involved in such a system should appear as less localized.

For N_{D3}, measurements were done at RT. Assuming that for N_{D3} all donors are very close to each other, we can base our interpretation of charging mechanism on an analogy to coupled donors in N_{D2} – case (B). We can expect that, for many interacting donors, charging appears as spatially uniform lowering of potential over

the doped area. This interpretation is in agreement with measured average potential depth of the channel in respect to the non-doped area while V_{sub} varies [as shown on Fig. 3-4(c)].

3.4 Conclusions

In summary, we characterized SOI-FETs with channels doped with different concentrations. KPFM measurements show systematic changes in dopant arrangement. We distinguish 3 main configurations: solitary donors, systems of a few coupled donors, and groups of many interacting donors. Depending on the concentration, dopants appear separated, grouped or in both configurations for intermediate concentrations. We also studied charging and discharging mechanism. At LT, electron filling appears as distinct neutralization of individual potential wells, but for coupled donors as a gradual screening due to addition of electrons. Similar results are shown for higher concentrations, when most dopants are close to each other. These observations give a direct insight into how dopants' arrangement depends on concentration and how charging mechanism for each identified donor-system works. Both are useful indications for the purpose of correlation of single-electron transport I-V characteristics with donor-induced potential landscapes.

.

4 Study of donor-induced quantum dots in Si nano-channels doped with different doping concentrations

This chapter is mainly based on:
K.Tyszka, D.Moraru, T.Mizuno, R.Jablonski and M.Tabe
Comparative study of donor-induced quantum dots in Si nano-channels by single-electron transport characterization and Kelvin probe force microscopy.
Journal of Applied Physics 117: 244307 (2015)

4.1 Introduction

Dopant atoms have been reported to work as quantum dots (QDs) in nanoscale-channel Si transistors, either individually, isolated from each other [17-21] or as clusters of a number of closely-located dopants [28,32]. Although several state-of-the-art techniques have been used to fabricate "dopant-atom" field-effect transistors (FETs) with precise positioning of one dopant [26] or a controlled number of dopants [24,61], uniformly- or selectively-doped channels with natural randomness of dopant configurations are generally studied because of the availability of conventional fabrication technologies. Donor-based FETs exhibit I-V characteristics with current peaks as a function of gate voltage (V_G), where each peak is ascribed to single-electron tunneling transport via an individual donor[17-22] or via clusters of donors[32,62]. With increasing V_G, such tunneling-transport features gradually disappear because of complex contributions in transport from multiple QDs and overlapping effects of ordinary FET diffusion current. Therefore, the first few current peaks are most sensitive to the lowest-energy potential landscape and can be considered most appropriate to study donor-induced QDs. Furthermore, the nature of such donor-induced QDs (due to a single donor-atom or due to a multiple-donor cluster) in different regimes of doping concentration has not yet been clarified.

In this chapter comparative study of the deepest-potential QD formed in nanoscale Si channels in a wide range of phosphorus (P) doping concentration is

described. We focus on two key aspects: (i) the first few current peaks in electron-tunneling transport as a function of V_G; (ii) direct observation and analysis of the potential landscapes observed by KPFM (see Chapter 2.1) in correlation with simulations (see Chapter 2.3). Here, we show I-V characteristics for devices with channels doped with P-donors below and above the metal-insulator transition (MIT) concentration, $N_D^{MIT} \approx 3.8\times10^{18}$ cm^{-3} (for details of fabrication see Chapter 2.2) Transport via donor-induced QDs in such devices is governed at low temperatures by Coulomb blockade, or single-electron tunneling. The I-V characteristics suggest that the deepest-potential QDs are mostly formed by individual P-donors (or clusters of a small number of P-donors) below the MIT concentration. On the other hand, above the MIT concentration, QDs are formed by a large number of P-donors clustered together. KPFM observations, correlated with simulations of dopant-induced potential landscapes, confirm the different nature of the QDs in these two regimes. Furthermore, it is found that, in highly-depleted channels, a single dominant QD can be formed with high probability, regardless of doping concentration. These findings provide fundamental knowledge about dopant-induced QDs, such as their potential profile and its impact on tunneling-transport characteristics.

4.2 Results and discussion

4.2.1 Single-electron transport characterization

Source-drain current (I_D) vs gate voltage (V_G) characteristics, together with possible P-donors' distributions and schematic channel potentials for two different SOI-FETs are shown in Figs. 4-1(a)-(b) and Figs. 4-2(a)-(b). These devices are representative for the two different regimes of concentration (N_D). I_D-V_G characteristics are measured at low temperature in order to avoid thermally-activated conduction and to promote single-electron tunneling as the dominant transport mechanism. For the low-concentration regime ($N_D \approx 1\times10^{18}$ cm^{-3}), a large

number of devices behave similarly to the example shown in Fig. 4-1(a), i.e., exhibiting isolated current peaks, with a simple structure, appearing at V_G's well below the threshold voltage of the FET channel. Since consecutive current peaks are not periodic and have irregular intensities, such current peaks are ascribed to different QDs. Therefore, each QD is expected to be formed by an individual P-donor [20]. In particular, the first observable current peak is attributed to tunneling via the deepest-potential QD, when its ground state is aligned with the Fermi level (E_F) of the source/drain leads by application of a certain V_G [31]. For V_G's lower than the peak voltage (region A), electrons are depleted from the QD (and, implicitly, also

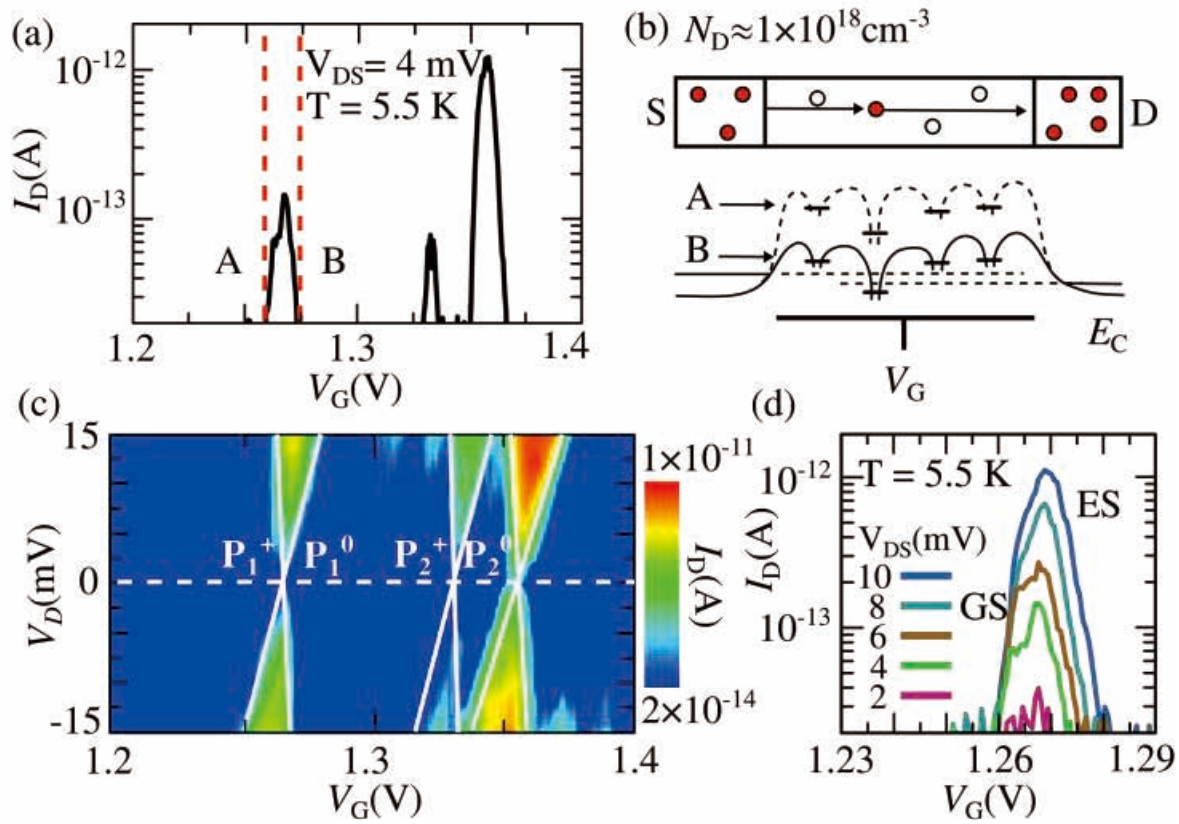

Fig. 4-1. (a) Low-temperature source-drain current (I_D) vs gate voltage (V_G) characteristics for an SOI-FET with the channel doped with P-donors at relatively low concentration ($N_D \approx 1\times10^{18}$ cm^{-3}). (b) One possible P-donors' distribution and schematic channel potential profiles. The first current peak, ascribed to single-electron tunneling via the deepest donor-induced QD, is marked by dashed lines separating two different V_G-regions, labeled A and B. (c) Stability diagram for this low-N_D SOI-FET, showing different Coulomb diamonds (marked by white boundaries) as signatures of tunneling via different P-donors (as marked in the figure). (d) V_{DS} dependence of the first current peak, exhibiting humps due to the ground state (GS) and due to the excited state (ES) of a P-donor.

from the channel), while for V_G's higher than the peak voltage (region B) one electron is captured into the QD. If the QD is formed by a single P-donor, the donor would be neutralized by capturing one electron and the successive current peak may be ascribed to another P-donor.

This interpretation is supported by the stability diagram shown in Fig. 4-1(c) and by the I_D-V_G curves measured as a function of V_{DS} shown in Fig. 4-1(d). Coulomb diamonds [23] observed in the stability diagrams (marked with solid white lines) are significantly different from each other. Such lack of periodicity suggests that each current peak (region between Coulomb diamonds) corresponds to different QDs, most likely to different individual, isolated P-donors, as labeled in Fig. 4-1(c). This is further confirmed by the I_D-V_G curves shown in Fig. 4-1(d) in which the sub-structure of the current peaks can be identified with increasing source-drain bias (V_{DS}). The main observed features, i.e., humps within the current peak, suggest tunneling transport via the ground state (labeled GS) and via a first excited state (labeled ES) of a single P-donor. By this analysis, we can conclude that each current peak can be assigned to a different P-donor working as QD, and, most importantly, that the first observable current peak is attributed to the tunneling via the deepest-potential QD.

For the high-concentration regime ($N_D \approx 1\times10^{19}$ cm^{-3}), typical observations are significantly different, as shown by the example in Fig. 4-2(a). As V_G is increased from low values (at which the channel is likely depleted of carriers, region A), single-electron tunneling transport gives rise to a current peak envelope. The current peak envelope contains a number of inflections and sub-peaks that suggest a dense spectrum of energy states in the transport-QD [as illustrated in Fig. 4-2(b)]. Such a complex spectrum is expected when the transport-QD is formed by a number of strongly-interacting P-donors, forming a molecule-like system which gives rise to bonding and anti-bonding states [32]. For V_G's higher than the first peak envelope (region B), one electron is captured in the QD. Hence, the following current peak envelope may be ascribed to a second-electron tunneling through the same QD with

one electron captured inside the QD.

Figure 4-2(c) shows the stability diagram corresponding to the I_D-V_G characteristics shown in Fig 4-2(a). In this diagram, an open-region can be first observed at lower V_G's. This is ascribed to the empty state of a donor-cluster QD. Then, one Coulomb diamond can be identified for higher V_G, in the range ~0.35-~0.55 V, most likely due to the stable charge state of the QD with one electron trapped inside. These structures appear as dominant before the onset of an increasing diffusion current (at even larger V_G's). It is natural to assume that the

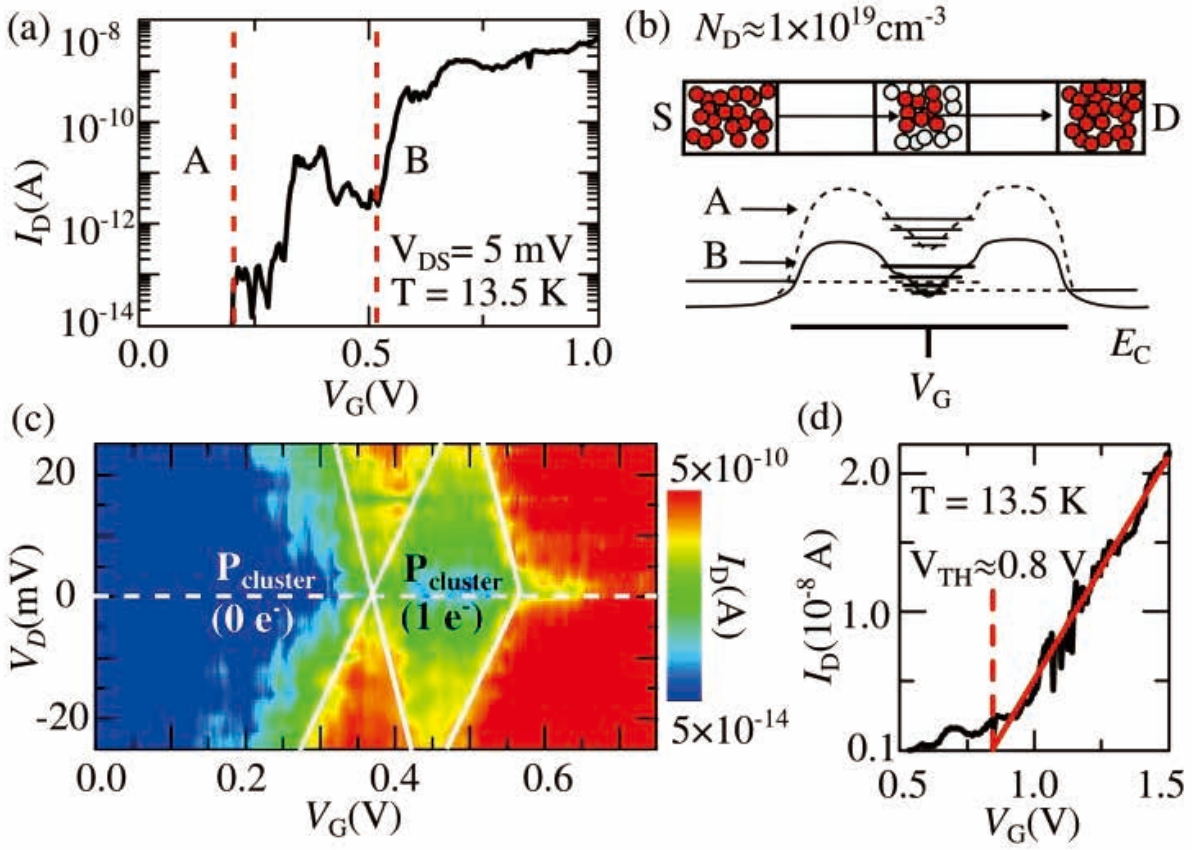

Fig.4-2. (a) Low-temperature source-drain current (I_D) vs gate voltage (V_G) characteristics for an SOI-FET with the channel selectively-doped with P-donors at relatively higher doping concentration (N_D≈1×10^{19} cm^{-3}). (b) One possible P-donors' distribution and schematic channel potential profiles. The first current peak envelope, ascribed to single-electron tunneling via the deepest-potential donor-cluster-induced QD, is marked by dashed lines, separating two different V_G-regions, labeled A and B. (c) Stability diagrams showing a Coulomb diamond as signature of tunneling via a donor-induced QD. (d) Approximate threshold voltage (V_{TH}) determination by fitting the linear region of the low-temperature I_D-V_G characteristics.

increasing current region marks approximately the threshold voltage (V_{TH}),[12] and the clear observation of a Coulomb diamond supports the model that tunneling occurs through discrete energy levels found below the conduction band. Alternatively, we roughly determine the threshold voltage (V_{TH}) to be ~0.8 V by fitting the linear region of the low-temperature I_D-V_G characteristics [as indicated in Fig. 4-2(d)]. Although this method is approximate due to the low temperature, it is reasonable to assume that any current peaks below this V_{TH} are due to tunneling via donor-states. It can be, thus, concluded that tunneling is the dominant transport mechanism at the initial stages of the I_D-V_G characteristics [Fig. 4-2(a)], and that the first current peak envelope is due to transport via a QD induced by a donor cluster.

Hence, the electrical characteristics shown in Figs. 4-1 and 4-2 suggest a different nature of the QD responsible for tunneling-transport for different doping concentration regimes. In order to further confirm the validity of this model, direct observation of donor-induced QDs is necessary. For this purpose, we study donor-induced potential landscapes by combining KPFM measurements and supporting simulations of thin Si channels doped in a wide range of doping concentration.

4.2.2 Correlated results of KPFM and simulations

Results of KPFM measurements (at room temperature, T=295 K) are shown in Fig. 4-3, while typical results of simulations are shown in Fig. 4-4. For purpose of this experiment the images were filtered with high-pass filter to remove long range potential fluctuations. This operation allows better observation of nanoscale features. For both experiment and simulation, the upper two images correspond to the low-concentration devices ($N_D \approx 1\times10^{18}$ cm^{-3}), while the lower two images correspond to the high-concentration devices ($N_D \approx 1\times10^{19}$ cm^{-3}). Images on the left are taken for negative substrate bias (V_{sub}=-4 V). For this case, by matching the amplitude of the observed potential variations in simulation, f_e was found to be 0% for $N_D = 1\times10^{18}$ cm^{-3} and 60% for $N_D = 1\times10^{19}$ cm^{-3}. Thus, for the higher-concentration KPFM devices, it is most likely that the channel was only partially depleted under the

application of V_{sub} = -4 V. This may be due to the larger channel area for these devices. The I-V devices, however, have smaller channels (on the order of 50×50 nm^2) and a top gate can be used to efficiently deplete the channel, so it is expected that full depletion (f_e=0%) can be readily obtained. Images on the right are for V_{sub} = 0 V which corresponds to channels fully screened by electrons (f_e=100%). Such condition corresponds to the high-V_G region in the I_D-V_G characteristics. In all KPFM and simulation images, darker contrast indicates lower electronic potential, i.e., regions which are more positively charged. For the devices doped below the MIT concentration, fine potential dips (5-10 nm in diameter, ~20 mV in depth) can be easily identified when electrons are depleted for V_{sub}=-4 V [Fig. 4-3(a)]. These fine features, also predominant in the simulation result [Fig.4-4(a)], are due to individual ionized P-donors (as also explained in more details in Chapter 3.2). In Figs. 4-3(a) and 4-4(a), although much fewer than the fine features, it is possible to also observe a few regions with larger extension (10-20 nm in diameter), numbered in the order of the potential depth. These are found to be clusters of 2-3 P-donors, when the P-donors are located at distances smaller than two Bohr radii from each other (r_B≈2.5 nm for P in Si[21-23]). Assuming a Poisson distribution of the donors, it can be estimated that there is ~8% probability to find a 2-donor cluster and ~1% probability to find a 3-donor cluster, i.e., ~90% probability to find QDs formed by isolated P-donor, which is consistent with our observation for the measured area (100×100 nm^2). Therefore, tunneling-transport is also expected to be mostly controlled by individual-donor-QDs. For V_{sub}=0 V in the KPFM image [Fig. 4-3(b)] and for full screening with electrons (f_e=100%) in the simulated image [Fig.4-4(b)], the majority of these fine features are smeared out.

For the devices doped above the MIT concentration, screening effects are more pronounced. Due to our specific design (selective doping) and low-dimensionality of the channels, high depletion of carriers is expected. However, the potential modulations observed in Fig. 4-3(c) for V_{sub}=-4 V are matched in simulation

when f_e is set to 60% [Fig. 4-4(c)], indicating that the channel is partially depleted. Even under this partial-depletion condition, the potential features can be clearly distinguished and analyzed. As observed in Fig. 4-3(c), the predominant type of

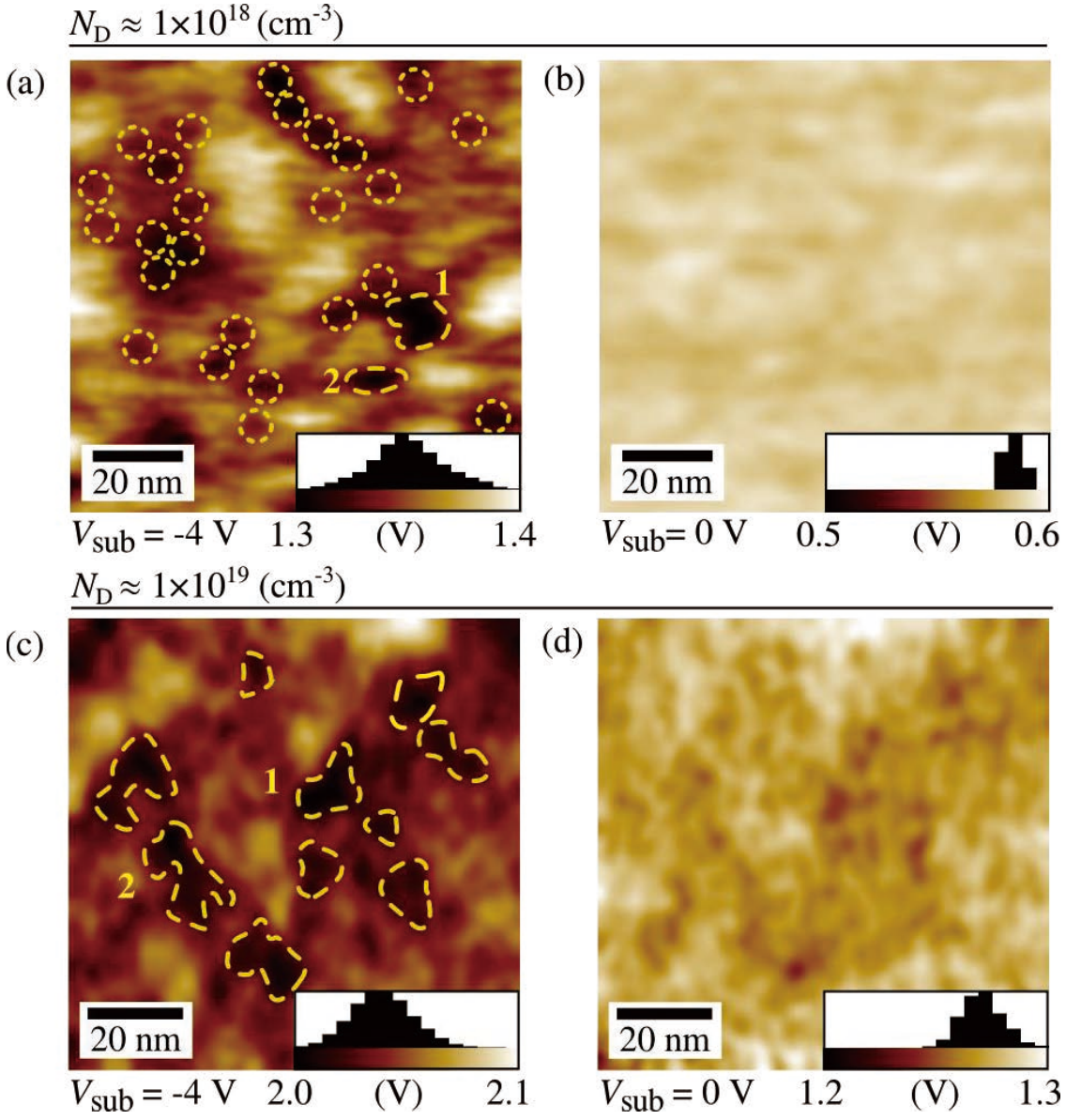

Fig. 4-3. Surface potential landscapes measured at room temperature for different concentrations (N_D) and substrate biases (V_{sub}). Images were filtered with high-pass filter. Potential range is indicated with histograms in the bottom-right corner of each image. (a) For low-concentration devices (N_D≈1×10^{18} cm^{-3}), V_{sub}=-4 V, single-P-donor QDs (fine circles) are predominant, while more extended, deeper features (irregular boundaries) are ascribed to 2-3 coupled P-donors. (b) For V_{sub}=0 V, these features are strongly screened by electrons. (c) For high-concentration devices (N_D≈1×10^{19} cm^{-3}), V_{sub}=-4 V, deep-potential areas (irregular boundaries) are ascribed to many-donors QDs. (d) These features are suppressed for V_{sub}=0 V due to electron screening. In (a) and (c), two deepest potential wells are numbered in the order of their potential depth.

features in this case are more extended areas (10-20 nm in diameter) with irregular boundaries and deeper potential (as also explained in more details in Chapter 3.2). This is also clearly observed in the simulated landscape shown in Fig. 4-4(c). Two deepest-potential wells are numbered in the order of their potential depth. Further

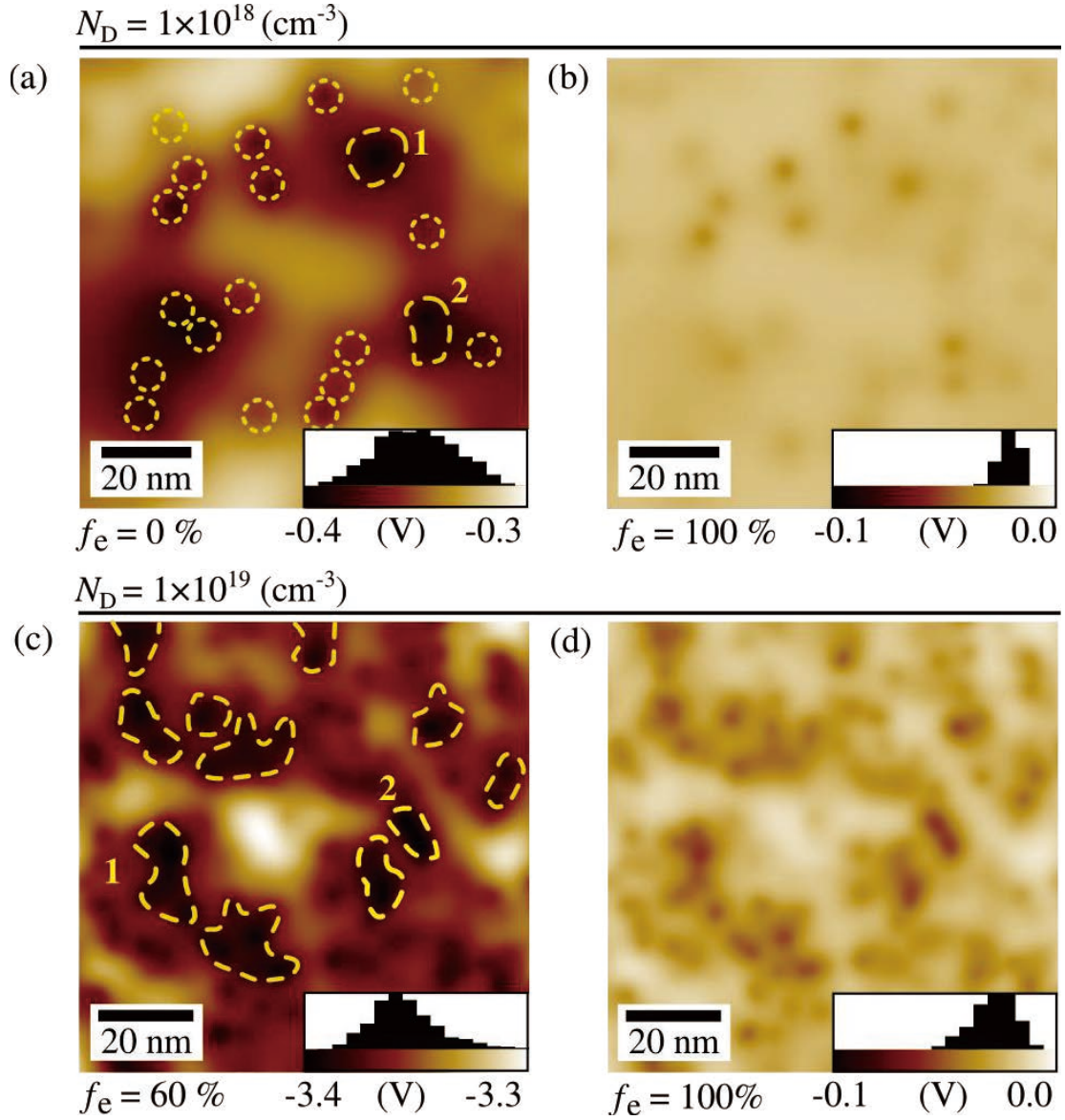

Fig. 4-4. Simulation results for different donor concentrations (N_D) and electron coverage fractions (f_e). Potential range is indicated with histograms in the bottom-right corner of each image. For low-concentration regime, fine features observed for f_e=0% [(a)] are marked similarly to Fig. 4-2(a). These features vanish for f_e=100% [(b)]. For high-concentration regime, deep-potential extended areas (marked by irregular dashed boundaries) can be observed as predominant for f_e=60% [(c)], while the fluctuations are suppressed for full screening, f_e=100% [(d)]. In (a) and (c), two deepest potential wells are numbered in the order of their potential depth.

analysis of simulated landscapes by simulation shows that these features are mostly given by clusters of 10-15 P-donors. Compared with these predominant features, finer features ascribed to individual P-donors are extremely rare. This suggests that the dominant QD in such a regime of concentration is definitely formed by a large number of P-donors (>10). For such high concentration ($N_D \approx 1\times10^{19}$ cm^{-3}), average inter-donor distance $d_{P\text{-}P}$ is smaller than $2\times r_B$ (in this case, ~4.6 nm). Hence, such agglomerations of many P-donors are reasonably expected [59,60]. Again, for V_{sub}=0 V in the KPFM image [Fig. 4-3(d)] and for the corresponding simulated image (f_e=100%) [Fig. 4-4(d)], the features are smeared out. However, a certain contrast still remains visible as a signature of the multiple-P-donor clusters. More detailed analysis of screening effects will be discussed in Fig.4-6.

The nature of the potential features observed for the depleted cases [Figs.4- 4(a) and 4-4(c)] is quantitatively described in Fig.4-5(a) for N_D=1×10^{18} cm^{-3} (f_e=0%) and in Fig. 4-5(b) for N_D=1×10^{19} cm^{-3} (f_e=60%). These figures show the

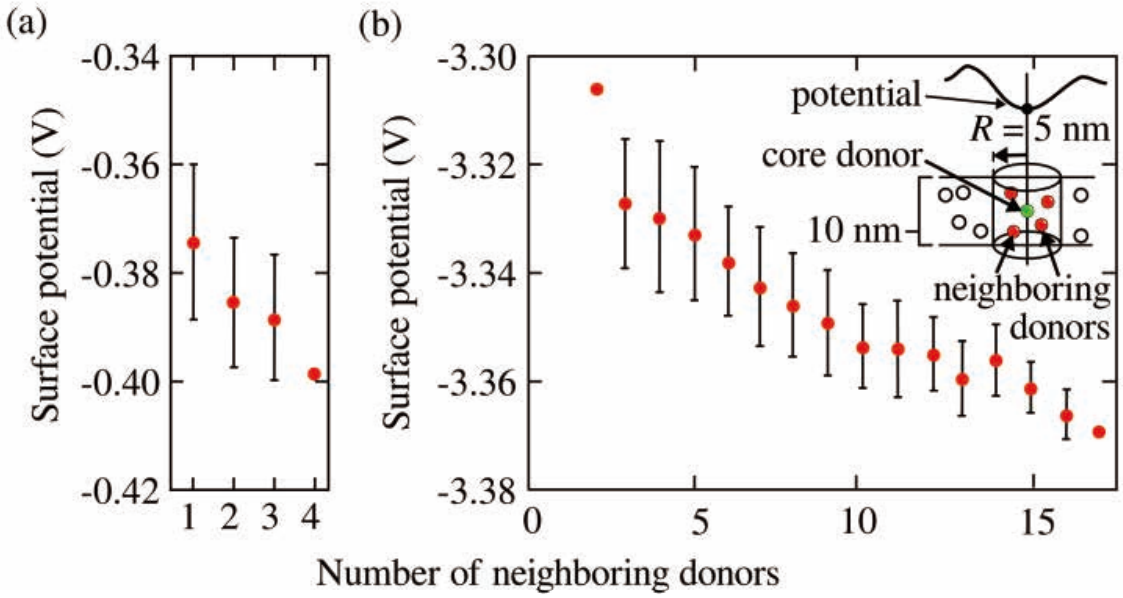

FIG. 4-5. Surface potential at different P-donor positions as a function of the number of neighboring P-donors for each core P-donor, with error bars showing standard deviation, for: (a) low concentration, N_D=1×10^{18} cm^{-3} (f_e=0%); (b) high concentration, N_D=1×10^{19} cm^{-3} (f_e=60%). The number of neighboring P-donors is calculated within a cylindrical volume with radius R=5 nm centered at the core P-donor, as shown in the inset. For the data points without error bars, only a single case was identified in the estimation area (100×100 nm^2).

relation between the surface potential (at the location of each P-donor) and the number of neighboring (clustered) P-donors significantly contributing to the potential well (within a radius R=5 nm, as illustrated in the inset). For both regimes, there is a clear correlation trend that deeper potential wells are statistically formed by clusters containing larger number of interacting P-donors. Below the MIT concentration [Fig. 5(a)], such clusters could be formed by at most 2-4 P-donors, although single P-donors remain statistically predominant in number [as visible in Fig.4-4(a)]. Above the MIT concentration [Fig. 4-5(b)], a large variation in the number of P-donors forming the clusters can be observed, in the range of 1-20 P-donors/cluster. Thus, for this high-concentration case, the potential landscape is defined by a combination of multiple-donor clusters with significantly different numbers of P-donors.

Finally, we focus on the analysis of the deepest-potential well, which corresponds to tunneling transport in the lowest-V_G range within a transport window V_{DS}=5 mV (in the range of typical source-drain bias used in the I_D-V_G characteristics shown in Fig. 4-1 and Fig. 4-2). The analysis process is schematically shown in the inset of Fig. 4-6(a). For this analysis, we simulated 50 different P-donors' distributions for different N_D's in the range 1×10^{17}~1×10^{19} cm^{-3}. Vertical axis shows the number of QDs (within the transport window) averaged for the results obtained from 50 samples. Electron coverage fraction (f_e) is indicated on the right. It can be seen that, in the entire range of concentrations, below and above the MIT concentration, a single dominant QD can be found with high probability (>50%) as long as we approach the condition of f_e=0%, i.e., for highly-depleted channels. For concentrations below the MIT concentration, it is easier to obtain highly-depleted channels and, therefore, we only focus on the case of f_e=0%. In this regime, isolated current peak observed at lowest V_G is ascribed to one dominant QD most likely formed by an individual P-donor. However, for the cases above the MIT concentration, increasing f_e leads to a rapid deterioration of the results and a larger

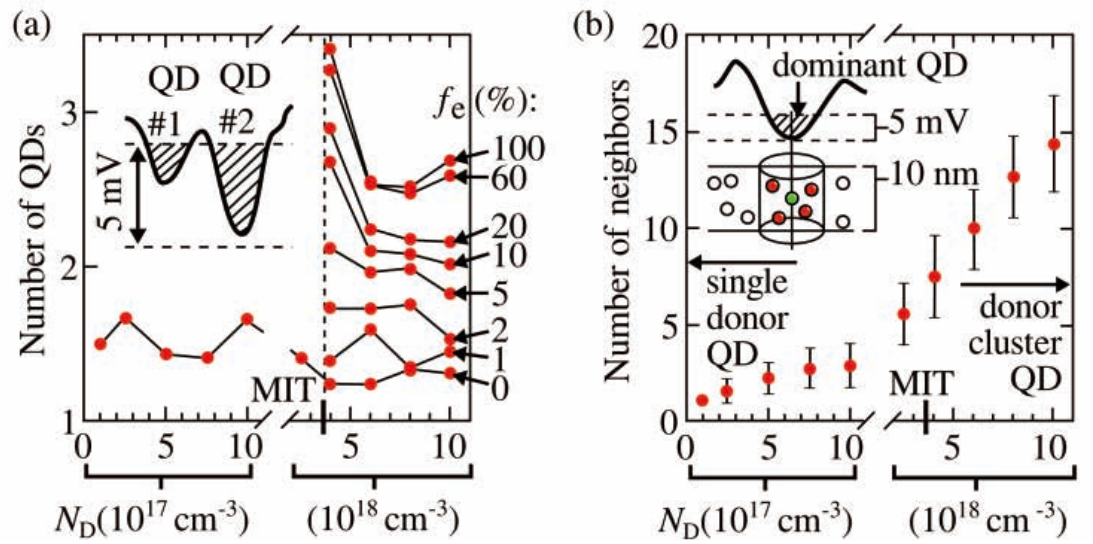

Fig. 4-6. (a) Average number of deepest-potential QDs within a V_{DS} window of 5 mV (as illustrated in the inset) as a function of donor concentration (N_D). 50 different P-donors' distributions were simulated for each N_D. For N_D above the metal-insulator transition (MIT) concentration, dependence on electron coverage fraction (f_e) is also shown. (b) Average number of P-donor neighbors forming the dominant QD for fully-depleted channels (f_e=0%) as a function of N_D. 50 samples (different donors' distributions) were simulated for each N_D. Inset: schematic calculation method for evaluating the number of neighboring P-donors contributing to the formation of each dominant QD, within a cylindrical volume of radius R=5 nm.

number of potential wells start to compete as dominant QDs. Nevertheless, for our small I-V devices, the channels can be highly-depleted at lowest V_G's, so the first current peak envelope can be ascribed to a single dominant QD. These results suggest that the full depletion favors the isolation of a single dominant QD in the entire wide range of doping concentrations studied here.

Since the first current peaks in the I_D-V_G characteristics correspond to single-electron tunneling in highly-depleted channels, in Fig. 4-6(b) the simulated number of P-donors forming the deepest-potential QD is plotted as a function of N_D. For this plot, f_e is set to 0%. Again, the results are averaged from 50 samples simulated for each N_D. The calculation procedure is illustrated in the inset of Fig. 4-6(b). Similarly to the case shown in Fig. 4-6(a), we used Bohr radius for P in Si to define the volume for the calculation. Therefore, the result shown here is directly related to the interactions between neighboring P-donors, which become significantly stronger

when the P-donors approach each other within a distance of 2 Bohr radii. Two significantly different behaviors can be identified, below and above the MIT concentration, labeled as “single-donor QD” and “donor-cluster QD” respectively. It can be seen that, for lower concentrations, the dominant QD is formed either by a single P-donor or by a small number of clustered P-donors (<4). For higher concentrations, however, a rapid increase in the number of P-donors/QD (>>5) can be observed. For both regimes, the internal structure of the QD differs not only in the number of donors forming the QD, but also in the degree of donor-donor interaction (related to the inter-donor distance). On average, increase of doping concentration leads to an increase of the number of dopants found inside the calculation volume and to a decrease of the inter-dopant distance, resulting in strengthening of dopant-dopant interactions. Therefore, higher doping concentration leads to a larger number of closely-placed and strongly-interacting donors within the QD. Thus, for concentrations well above MIT, even a small change in the concentration significantly affects the number of donors forming the dominant QD and the distance between donors. Hence, it can be concluded that the configuration of P-donors that give rise to the deepest QD in this regime is highly sensitive to doping concentration, suggesting that the internal structure of the QD can be statistically tuned by changing N_D.

These results provide evidence of the different nature of the QDs responsible for transport in the I_D-V_G characteristics. For low donor-concentration, tunneling-transport predominantly takes place via single P-donors, although clusters of a small number of P-donors cannot be excluded. For higher concentration, however, the complex current peak envelope [shown in Fig. 4-2(a)] is due to the tunneling-transport via a cluster-QD formed by many closely-placed P-donors. In this way, the intrinsic nature and composition of the QDs can be correlated with the basic features of the I-V characteristics, offering a pathway to understanding the fundamental properties of dopant-induced QDs in different regimes of interaction.

4.3 Conclusions

For the first time, an experimental correlation between single-electron tunneling characteristics and potential landscapes induced by P-donors in nanoscale-channel SOI-FETs, as measured by KPFM, in a wide range of doping concentration. It is found that, below and above metal-insulator transition concentration, the nature of the QDs is significantly different, defined by: individual donors below MIT and clusters of a large number of donors above MIT. Most importantly, however, for highly-depleted channels, only one dominant, deepest-potential QD may be formed with high probability for the entire range of doping concentration. These findings provide insights for designing optimized dopant-based devices in which either single dopants or clusters of many dopants can be utilized as dominant quantum dots.

5 Effect of selective doping on the spatial dispersion of donor-induced quantum dots in Si nanoscale channel

This chapter is mainly based on:
K.Tyszka, D.Moraru, T.Mizuno, R.Jablonski and M.Tabe
Effect of selective doping on the spatial dispersion of donor-induced quantum dots in Si nanoscale transistors. To be published in Applied Physics Express 8 (2015)

5.1 Introduction

In dopant-atom transistors, individual dopant atoms [17-21] or clusters of a few dopants [28,32,62], work as quantum dots (QDs) in nanoscale channels, giving rise to single-electron tunneling current peaks. Dopant-atom transistors have been proposed in a variety of designs, but generally are affected by the random placement of dopants. Control of position and number of dopant-induced QDs remains a challenging task and for practical applications, it is essential to clarify the key factors that affect the dispersion of donor-induced QD positions and to investigate the possibility to control such factors. Furthermore, until now, current peaks due to donor-QDs have not been directly correlated with measured donor-induced potentials.

In this chapter, we study such correlation by investigating the impact of doping concentration and selective doping pattern (see Chapter 2.2) on the spatial dispersion of donor-induced QDs in the channels of nanoscale transistors. For that purpose, we combine KPFM measurements (for details on KPFM see Chapter 2.1), supported by potential simulations (for details see Chapter 2.3), with low-temperature electrical characterization of donor-atom single-electron tunneling transistors. In previous Chapter 4, it was shown that in the low-concentration regime, transport-QDs are dominantly formed by individual donors. In the high concentration regime, clusters formed by multiple donors appear as dominant QDs in transport. It is found that a macroscopic U-shaped potential, most prominent in the case of high-concentration selectively-doped transistors, favors the formation of

donor-induced QDs near the center of the channels. These results allow a correlation between potential landscapes, as measured by KPFM, and single-electron tunneling transport, as observed in the low-temperature I-V characteristics.

5.2 KPFM results and discussion

KPFM results obtained at room temperature for an SOI-FET doped with low concentration ($N_D \approx 1\times10^{18}$ cm^{-3}) are shown in Fig. 5-2(a). For these measurements, V_{sub}=-4 V, so it can be assumed that electrons are removed and P-donors remain ionized in the channel. Fine potential modulations can be observed within the 100×100 nm^2 observation area. In order to observe the evolution of these features, in the line profiles shown in the right panel, V_{sub} is changed as a parameter. It can be seen that the potential minimum significantly changes position for different V_{sub}, suggesting that the position of the QD is sensitive to the applied bias. Figure 5-2(b) shows surface potential simulated for an electron coverage fraction (f_e) of 0% (fully-depleted channel) both as potential landscape (left) and as line profile (right panel). Similar features (fine modulations) as in the experimental data are due to different individual P-donors.

For devices with channels doped with higher concentration ($N_D \approx 1\times10^{19}$ cm^{-3}), surface potential landscapes measured by KPFM at room temperature and simulated using our procedure are shown in Fig. 5-3. The channels are doped using a selective-doping technique, in which a heavily-doped central region is isolated from source and drain leads by nominally non-doped gaps. This design allows for the quasi-metallic channel to be depleted by applying V_{sub}. First of all, it can be observed that the macroscopic potential contrast is significantly enhanced as compared with lower-concentration devices (shown in Fig. 5-2). Moreover, within the selectively-doped area, several regions with deeper potentials and with relatively irregular shapes are formed. For V_{sub}=-4 V, corresponding to the potential landscape shown in

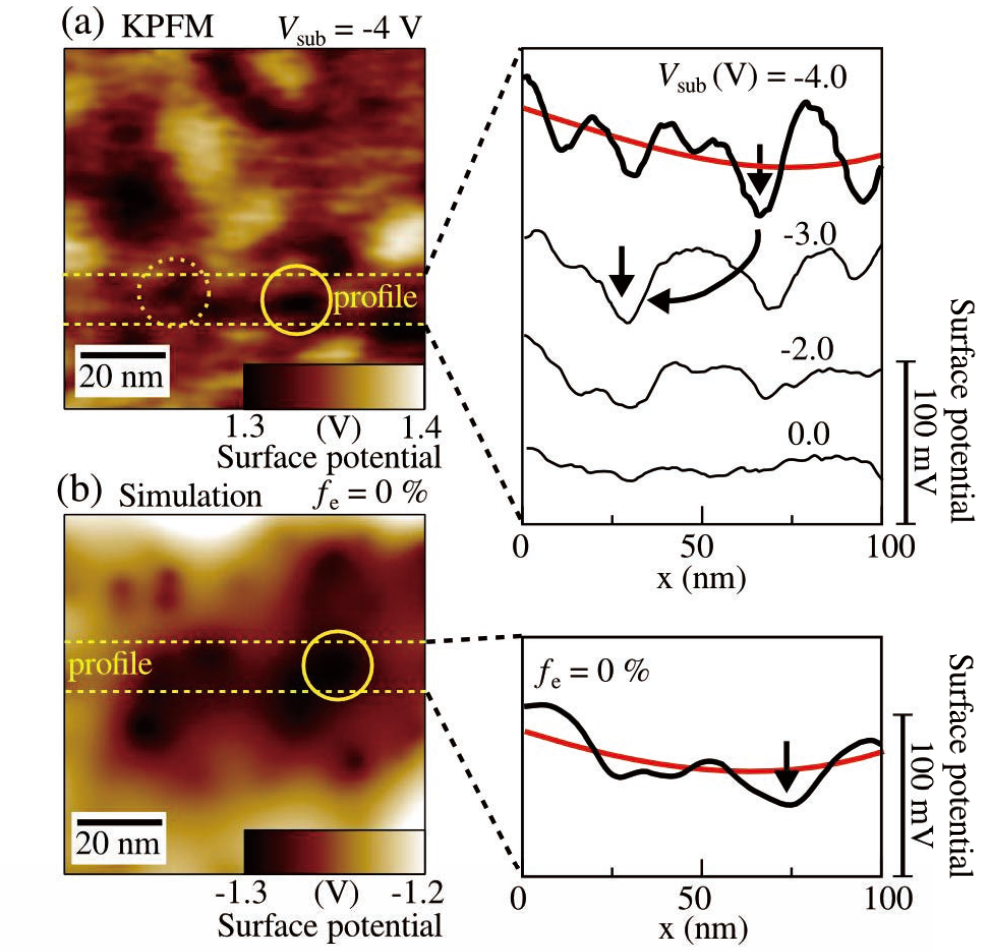

Fig. 5-2. (a) Surface potential of the channel of an SOI-FET doped with low concentration (N_D≈1×10^{18} cm^{-3}) measured by KPFM at room temperature. Potential range is indicated by the scale bar. Right panel: Line profiles in the marked area as a function of V_{sub} (-4.0~0.0 V). Significant changes of the potential minimum position can be observed by increasing V_{sub} (as indicated for V_{sub}=-3.0 V). (b) Example of simulated donor-induced potential landscape for channels doped with low concentration (N_D≈1×10^{18} cm^{-3}) for f_e=0% (fully-depleted channel). Right panel: line profile along the marked area, indicating the channel potential minimum.

Fig. 5-3(a), a large amount of electrons are expected to be depleted from the channel and only one such low-potential region becomes a dominant QD (as marked in the figure). Line profiles shown in the right panel illustrate the evolution of the potential minimum as a function of V_{sub}. It can be seen that, even with increasing V_{sub} in the positive direction, the potential minimum remains localized in the same area, relatively close to the center of the channel. Figure 5-3(b) shows an example of simulated potential landscape for high-concentration channels, assuming an

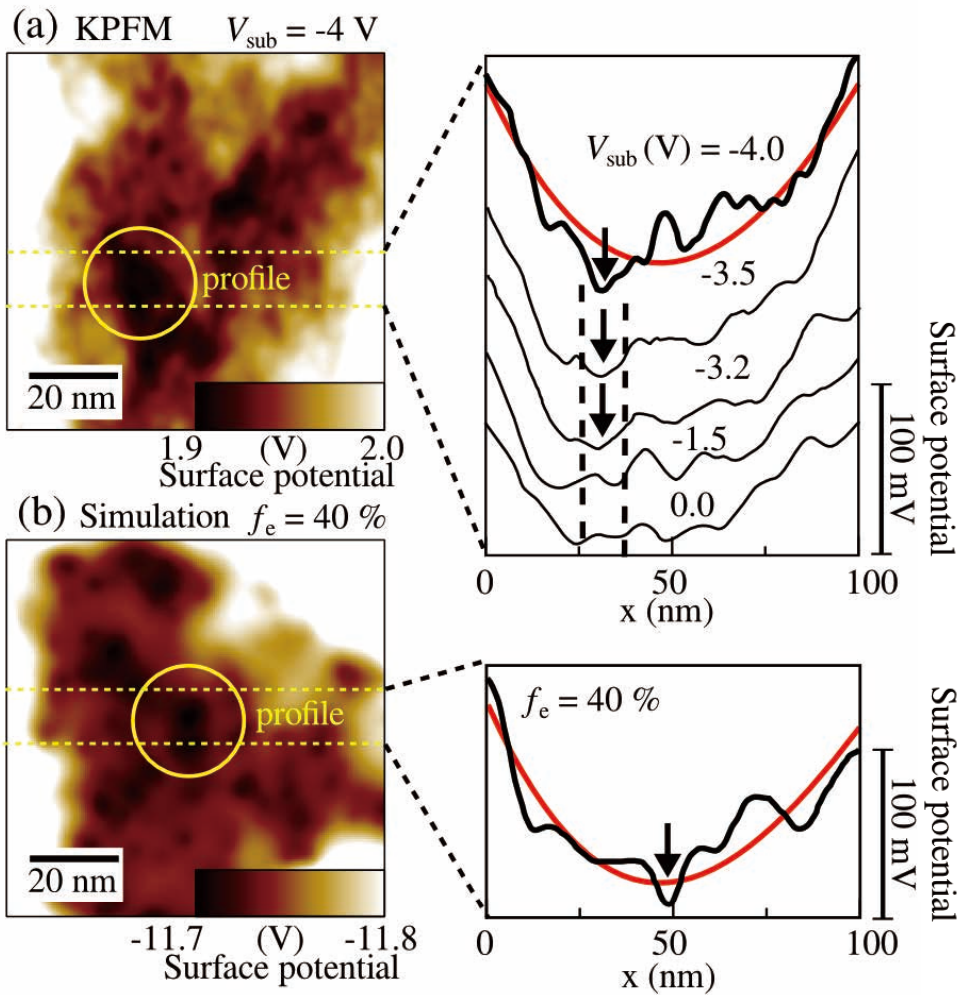

Fig. 5-3. (a) Surface potential of the channel of an SOI-FET doped with high concentration (N_D≈1×10^{19} cm^{-3}) measured by KPFM at room temperature. Potential range is indicated by the scale bar. Right panel: Line profiles in the marked area as a function of V_{sub} (-4.0~0.0 V), rescaled for visibility. Potential minimum remains localized in the same area for a wide range of V_{sub}, as marked by the arrows. (b) Example of simulated donor-induced potential landscape for high concentration (N_D≈1×10^{19} cm^{-3}) for f_e=40% (partly-depleted channel). Right panel: line profile along the marked area (rescaled for comparison with experiment), indicating the channel potential minimum.

electron coverage fraction (f_e) of 40% (partly-depleted channel). Low-potential regions, similar to the ones observed in the experimental data, can be also identified in the simulated landscapes and are ascribed to clusters of multiple strongly-coupled P-donors found close to each other. A more detailed analysis of the nature of such multiple-donor clusters was presented in previous Chapter 4. From these results, it can be noted that, different from the case of low-concentration devices, a

macroscopic U-shaped potential appears as a background profile. This can be more easily observed for highly-depleted channels (V_{sub}=-4 V), in the upper profile of the right panel. This potential background is induced by selective doping and by the large number of P-donors defining the potential. These findings suggest that the macroscopic profile may significantly contribute to a more centralized position of low-potential QDs in the channel.

In order to understand this effect more quantitatively, we performed a statistical analysis based on simulations of potential landscapes for a number of 50 samples for different N_D values [Fig. 5-4(a)]. In previous Chapter 4 we showed that, within a small potential window measured from the minimum potential in the channel, there will generally be only one area with the lowest potential, i.e., only one dominant QD. We evaluated the distance between such a dominant-QD and the center of the sample (D) as illustrated in the inset of Fig. 5-4(a). For low-N_D (and f_e=0%), the deviation of the dominant-QD from the center is remarkable, confirming the interpretation based on Fig. 5-2 that the QDs are relatively scattered within the channel. For higher-N_D (and f_e=0%), the dominant-QD appears significantly closer to the channel center. This supports our interpretation based on the data shown in Fig. 5-3, that high-N_D selectively-doped channels benefit from a macroscopic potential background to form the QD with better control near the channel center. Increasing f_e leads to an increasingly larger deviation of the QD position from the center of the channel. This effect can be attributed to the flattening of the macroscopic U-shaped potential background due to enhanced electron screening. This analysis has direct implications for the interpretation of single-electron tunneling transport in donor-induced QDs.

The typical dimensions of FET channel are in range of deca-nanometers, therefore, to address more realistic structures of the FET's, in Fig. 5-4(b), we plot the dependence of potential minimum offset on the sample area, for range of concentrations. Here, we focus on f_e = 0% only, as for a smaller channel dimensions

full depletion is expected. Although the tendency is similar as in Fig. 5-4(a), for smaller *A*'s the effect of favoring of central QD position is weakened due to decreasing of total number of donors per volume. Nevertheless, it is still prominent for high concentrations.

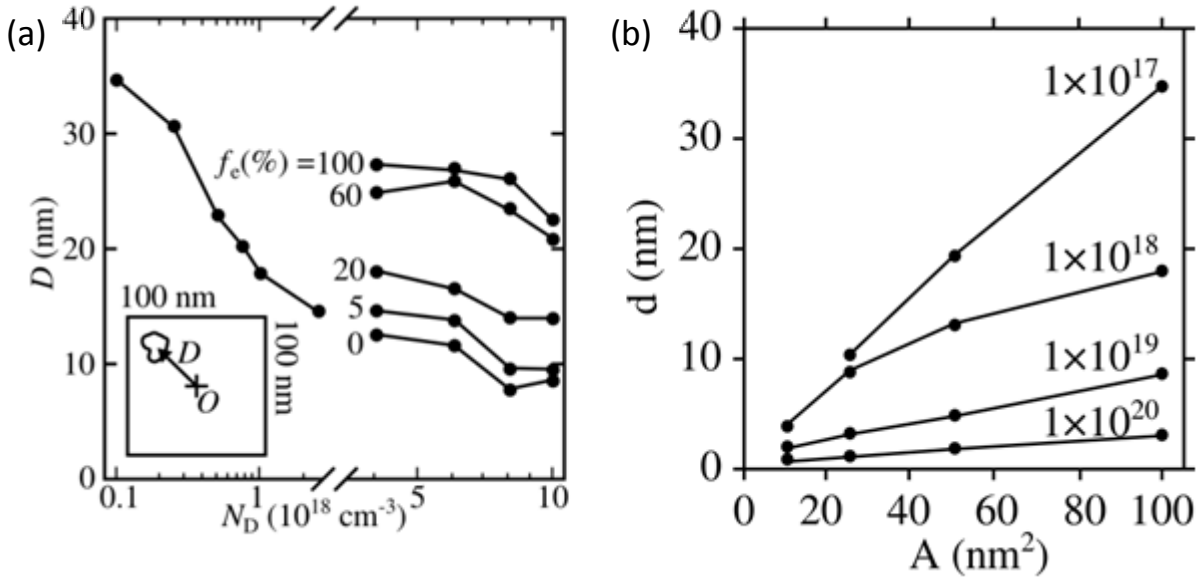

Fig. 5-4. Statistical simulation of average distance (*D*) between the dominant donor-induced QD (lowest potential in the channel) and channel center as a function of N_D (as illustrated in the inset). (a) Average *D* is obtained for each N_D from 50 samples (having areas of 100×100 nm^2) with random distributions of P-donors. The effect of f_e (increasing screening) is shown for high-N_D regime; for low-N_D regime, f_e=0%. (b) The dependence of potential minimum offset on the sample area, for range of concentrations.

5.3 KPFM and I-V correlation

In order to illustrate the correlation between donor-induced potential landscapes and I-V characteristics, we investigated SOI-FETs with smaller channels (width and length on the order of 50-100 nm) doped under similar conditions as the KPFM devices, but having a top Al gate. Measurements were taken at small source-drain biases (V_{DS}≈5 mV) and at low temperatures (T<15.0 K) in order to clearly observe signatures of single-electron tunneling transport in the I_{DS}-V_{FG} characteristics. Measurement results for representative devices from low-N_D and high-N_D regimes are shown in Fig. 5-5 and Fig. 5-6 respectively. Although

temperature is slightly different, it does not affect the comparison of the two sets of data. The electrical characteristics (I_{DS}-V_{FG} characteristics and stability diagrams, i.e., plots of I_{DS} in the V_{DS}-V_{FG} plane) are correlated with simulations of potential landscapes for increased electron screening and with estimated energy spectra expected within the transport-QD.

For the low-N_D regime, the I_{DS}-V_{FG} characteristics exhibit isolated current peaks, with irregular periods and intensities. These are usually ascribed to different, individual P-donors (as labeled in Fig. 5-5(a) for P_1, P_2, and P_3). In order to confirm this interpretation, we measured the stability diagram, as shown in Fig. 5-5(b). Low-current regions (below noise level, ~20 fA) are delineated by white boundaries to define the Coulomb diamonds formed between successive current peaks. At high V_{DS} (dashed boundaries) the behavior is more complex, possibly because several P-donors may appear in the V_{DS}-window and contribute to transport. However, in the low-V_{DS} region (solid boundaries), tunneling transport is expected to be due to a single QD. Based on this consideration, we performed a quantitative analysis of the slopes of Coulomb diamonds in low-V_{DS} region in order to evaluate the parameters associated with each QD. From adjacent slopes, we can evaluate the lever-arm factors, $\alpha=C_G/C_\Sigma$, where total capacitance is $C_\Sigma=C_S+C_D+C_G$, with C_S, C_D, C_G being the capacitance between the transport-QD and source, drain, gate, respectively. For the first 3 peaks, we found lever-arm factors α of 0.43, 0.64, and 0.51 (±0.01), respectively. These results suggest that successive peaks are due to QDs with different couplings to the gate. Lateral location of the QD along the channel was also evaluated based on the C_D/C_S ratio extracted from the slopes; for the first 3 peaks, C_D/C_S values are approximately 0.24, 0.30, and 0.55. This shows that the QD location changes along the source-drain direction for successive peaks. This analysis supports our model that each current peak is due to a different individual P-donor. Simulated potential landscapes [Fig. 5-5(c)] consistently show that the lowest-potential region is dominated by sharp potential wells, due to different P-donors. Successive

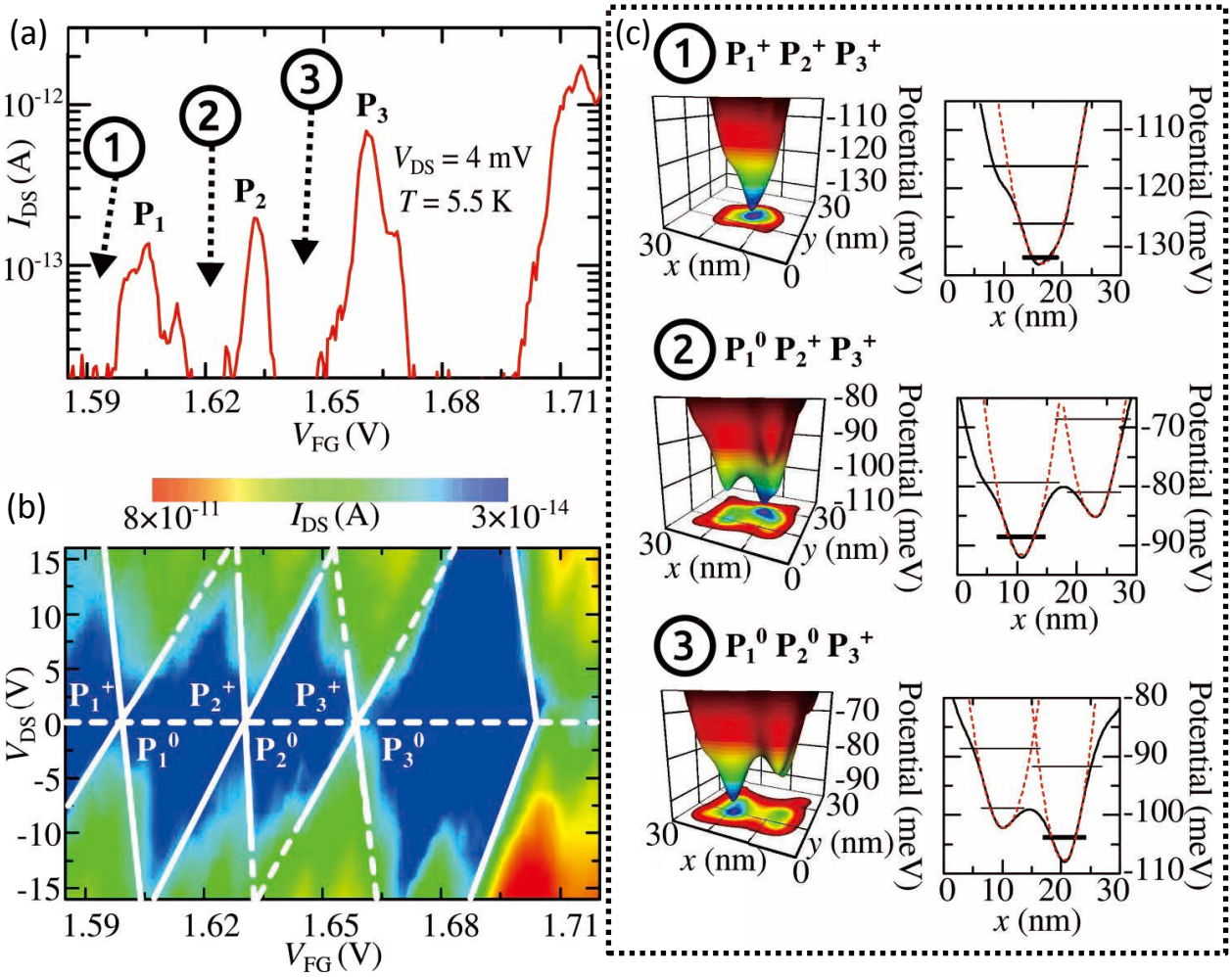

Fig. 5-5. (a) I_{DS}-V_{FG} characteristics and (b) stability diagrams (I_{DS} plots in V_{DS}-V_{FG} plane) measured at low temperature, correlated with simulated potential landscapes and energy (c) spectra of the transport-QD for low-concentration devices (N_D≈1×10^{18} cm^{-3}). The isolated current peaks in I_{DS}-V_{FG} characteristics are ascribed to different P-donors [as labeled]. Analysis of slopes in stability diagram indicates different positions of the P-donors within the channel. Position of the transport-QD changes significantly by neutralization of consecutive P-donors [as shown in left panels of (c)], while ground-state energy level is always localized in the area of individual P-donors [as shown in right panels (c)].

landscapes are simulated after neutralizing the deepest-potential P-donors one by one. A simplified calculation of energy levels in such QDs was done by treating the QDs as 1D square potential wells, leading to energy spectra as shown in Fig. 5-5, right panels. It can be seen that at least the ground-state level is localized within the potential well defined by individual P-donors.

The situation is significantly different for the high-N_D case (in Fig. 5-6). I_{DS}-V_{FG} characteristics measured at low temperature, shown in Fig. 5-6(a), exhibit current

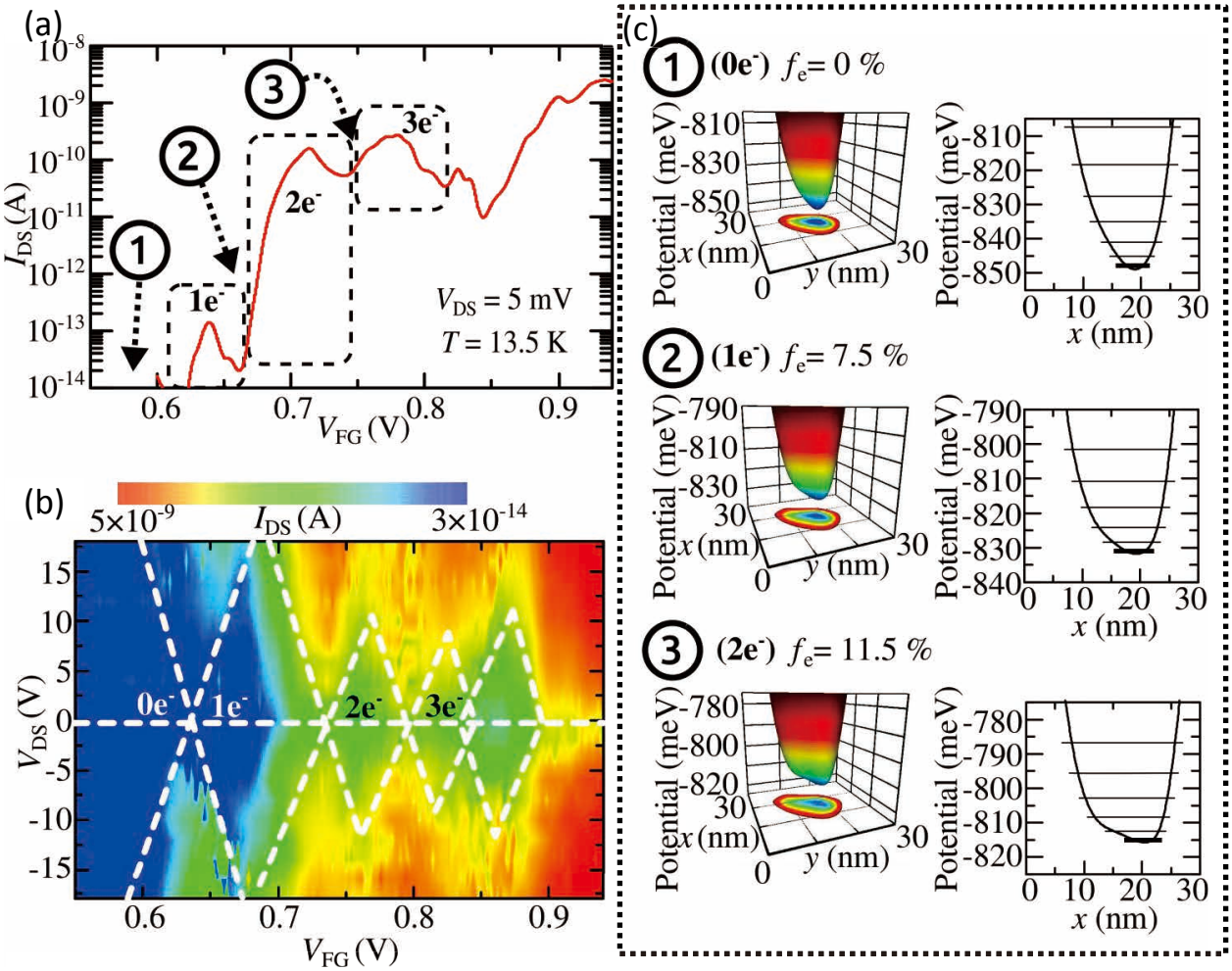

Fig. 6-5. (a) I_{DS}-V_{FG} characteristics and (b) stability diagrams (I_{DS} plots in V_{DS}-V_{FG} plane) measured at low temperature, correlated with (c) simulated potential landscapes and energy spectra of the transport-QD for high-concentration devices (N_D≈1×10^{19} cm^{-3}) in lower panels. The successive current peaks are ascribed to single-electron tunneling via a unique multiple-donor cluster-QD. Stability diagrams exhibit multiple Coulomb diamonds, but at different current levels because of a large background current. By increasing screening in the channel, as shown in, the transport-QD remains localized near channel center [left panels, (c)] and dense energy levels are expected [right panels, (c)].

peak envelopes, rather than isolated, sharp current peaks. Typical characteristics for devices of this type show also a rapid increase of the FET current in the background, which makes the detailed analysis of the stability diagrams more complex. However, from the stability diagram shown in Fig. 5-6(b), despite the presence of the background FET current, several consecutive Coulomb diamonds with similar features can be noticed. This suggests multiple-electron occupancy of the same QD [as marked in the figures Fig. 6-5(a),(b)]. According to study in Chapter 4, such QD is

due to the strong interaction of a number of P-donors located close to each other, forming a multiple-donor cluster-QD. Such interpretation is also supported by the potential simulations shown in Fig. 6-5(c)-left panels. Starting from the full-depletion (f_e=0%) condition, the lowest-potential region is dominated by a unique potential well for a significant range of electron screening. This suggests that, even by adding electrons into the QD, the location of the transport-QD does not significantly change. We also evaluated the energy levels of such QDs, again treated in a first approximation as 1D potential wells. The energy spectra are illustrated in the right sub-panels of Fig. 5-6(c) for consecutive potential wells, obtained by changing the electron screening level in the channel. Relatively denser energy spectra can be observed, consistent with the fact that current envelopes typically embed a number of inflections or sub-peaks [32]. Alternatively, the sub-structure of the current envelopes can also be ascribed to the molecular interactions among neighboring P-donors within the multiple-donor cluster. The results shown here suggest the impact on the single-electron tunneling characteristics due to multiple-donor clusters that form QDs relatively stable as a function of V_G. At higher V_G (higher f_e levels), more complex features start to be observed due to the interaction of several cluster-QDs, as well as due to the gradual opening of the FET-channel conduction.

The results shown in Fig. 5-5 and 5-6 illustrate an approach to correlate the potential landscapes induced by P-donors in nano-channels with single-electron tunneling characteristics. Such interpretation, mediated by a statistical analysis of simulated potential landscapes and energy spectrum evaluation, can provide a breakthrough in the study of donor-induced QDs. By understanding the key factors that contribute to an enhanced control of the position of donor-induced QDs, the design of donor-atom nanoscale transistors can be optimized for more robust operation, aiming toward high-temperature tunneling operation.

5.4 Conclusions

In summary, we studied the main factors that affect the spatial dispersion of donor-induced QDs in the channels of Si nano-FETs. From KPFM measurements, combined with simulations of donor-induced potential landscapes, we found that, for channels selectively-doped with relatively high concentration, a macroscopic U-shaped potential background becomes prominent, favoring a centralized location of the dominant QD near the center of the channel. Donor-induced potential landscapes have been correlated with I-V characteristics of donor-atom transistors in different regimes of doping concentration, illustrating the possibility to control different types of donor-induced QDs, either due to individual P-donors, or due to clusters of several P-donors.

6 Summery

For the first time, experimental correlation between single-electron tunneling characteristics and potential landscapes induced by P-donors in nanoscale-channel SOI-FETs, in a wide range of doping concentration was presented. The main factors that affect the spatial dispersion of donor-induced QDs in the channels of Si nano-FETs were also studied. Most importantly, it was found that, for highly-depleted channels, only one dominant, deepest-potential QD may be formed with high probability for the entire range of doping concentration. For high concentrations above MIT the internal structure of such QD strongly depends on concentration. From KPFM measurements, combined with simulations of donor-induced potential landscapes, it was found that, for channels selectively-doped with relatively high concentration, a macroscopic U-shaped potential background becomes prominent, favoring a centralized location of the dominant QD near the center of the channel.

These findings provide insights for designing optimized dopant-based devices in which either single dopants or clusters of many dopants can be utilized as dominant quantum dots. It is expected that further optimization of such device parameters like channel size, shape and doping profile can lead to further enhancement or maybe even full control over donor-induced QD formation in dopant-atom devices fabricated by means of classical CMOS processes.

References

1. G.E. Moore, Cramming more components onto integrated circuits, Electronics, pp.114-117 (1965).
2. Cited in: Moor's law keeps going, defying expectations, Scientific American, 19 May 2015 (internet source: www.scientificamerican.com)
3. International Technology Roadmap for Semiconductors, Executive Summary, 2013 Edition, Table ORTC1, p.17 (internet source: www.itrs.net)
4. R. Keyes, The effect of randomness in the distribution of impurity atoms on FET thresholds. Appl. Phys. **8**, 251-259 (1975)
5. T. Mizuno et al., Experimental study of threshold voltage fluctuations due to statistical variation of channel dopant number in MOSFET. IEEE Trans. Electron Devices **41**, 2216-2221 (1994).
6. A. Asenov, Random dopant induced threshold voltage lowering and fluctuations in Sub-0.1 m MOSFET's: a 3-D "atomistic", simulation study. IEEE Trans. Electron Devices **45**, 2505 (1998)
7. H. Wong et al., Discrete dopant distribution effects in nanometer-scale MOSFETs. Microelectron. Reliab . **38**, 1447-1456 (1998)
8. P. Ebert et al., Nanoscale fluctuations in the distribution of dopant atoms: dopant-induced dots and roughness of electronic interfaces. J. Vac. Sci. Technol. B **22**, 2018-2025 (2004)
9. T. Shinada et al., Enhancing semiconductor device performance using ordered dopant arrays. Nature **437**, 1128-1131 (2005).
10. F. Shwierz, *Graphene transistors.* Nat. Nanotech. **5**, 487 (2010)
11. M. Kastner, *The single-electron transistor*. Rev. Mod. Phys. **64**, 849-858 (1992).
12. H. Zeller, I. Giaver, *Tunneling, Zero-Bias Anomalies, and Small Superconductors* . Phys. Rev. **181**, 789 (1969).
13. J.H.F Scott-Thomas, *Conductance Oscillations Periodic in the Density of a One-Dimensional Electron Gas*. Phys. Rev. Lett. **62**, 583 (1989).

14. J.S. Shin et al., *Room-temperature charge stability modulated by Quantum effects in a nanoscale silicon island.* Nano Lett. **11**, 1591 (2011)

15. A. K. Geim et al., *Fermi-edge singularity in resonant tunneling*, Phys. Rev. Lett. **72**, 2061 (1994).

16. M. R. Deshpande et al., *Spin Splitting of Single 0D Impurity States in Semiconductor Heterostructure Quantum Wells*. Phys. Rev. Lett. **76**, 1328 (1996).

17. H. Sellier et al., *Transport Spectroscopy of a Single Dopant in a Gated Silicon Nanowire*. Phys. Rev. Lett. **97**, 206805 (2006).

18. Y. Ono et al., *Conductance modulation by individual acceptors in Si nanoscale field-effect transistors.* Appl. Phys. Lett. **90**, 102106 (2007).

19. G.P. Lansbergen et al., *Gate-induced quantum-confinement transition of a single dopant atom in silicon FinFET* Nature Phys. **4**. 656 (2008).

20. M. Tabe et al., *Single-electron transport through single dopants in a dopant-rich environment*. Phys. Rev. Lett. **105**, 0160803 (2010)

21. M. Pierre et al., *Single-donor ionization energies in a nanoscale CMOS channel*. Nat. Nanotechnol. **5**, 133 (2010)

22. P. M. Koenrad, M.E. Flate, *Single dopants in semiconductors*. Nature Mat. **10**, 91 (2011).

23. F. Zwanenburg et al, *Silicon quantum electronic*. Rev. of Mod. Phys. **85**, 961 (2013).

24. E. Prati et al., *Anderson-Mott transition in arrays of a few dopant atoms in a silicon transistor.* Nature Nanotechnol. **7**, 443 (2012).

25. A. Fuhrer et al., *Atomic-scale, all epitaxial in-plane gated donor quantum dot in silicon.* Nano Lett., **9**, 707-710 (2009).

26. M. Fuechsle et al., *A single-atom transistor*. Nature Nanotechnol. **7**, 242 (2012).

27. B. Weber et al., *Engineering independent electrostatic control of atomic-scale (~4nm) silicon double quantum dots*. Nano Lett. **12**, 4001-4006 (2012).

28. B. Weber et al., *Spin blockade and exchange in Coulomb-confined silicon*

double quantum dots. Nature Nanotechnol. **9**, 430 (2014) .

29. H.Büch et al., *Spin readout and addressability of phosphorous-donor clusters in silicon*. Nature Com. **4**, 2017 (2013).
30. T.F Watson et al., *Transport in asymmetrical coupled donor-based silicon triple quantum dot.* Nano Lett. **14**, 1830-1835 (2014) .
31. E. Hamid et al., *Electron-tunneling operation of single-donor-atom transistors at elevated temperatures*. Phys. Rev. B **87**, 085420 (2013).
32. D. Moraru et al., *Transport spectroscopy of coupled donors in silicon nano-transistors*. Sci. Rep. **4**, 6219 (2014).
33. E.W. Wogel, *Technology and metrology of new electronic materials and devices.* Nature **2**, 25-32 (2007).
34. D. K. Schroeder, *Semiconductor Material and Device Characterization*, 3rd ed., John Wiley and Sons, New Jersey (2006).
35. G. E. McGuire, *Characterization of Semiconductor Materials: Principles and Methods*. vol.**1**, Noyes Publications, New Jersey (1989).
36. S. Kalinin, *Scanning Probe Microscopy – electrical and electromechanical phenomena at the nanoscale.* vol.2, Springer Science, New York (2007)
37. J.Hwang et.al., *Three-Dimensional Imaging of Individual Dopant Atoms in $SrTiO_3$* , Phys. Rev. Lett. **111**, 266101 (2013)
38. A.K. Kambham et al., *Atom probe for finFET dopant characterization*. Ultramicroscopy **111** , 535-539 (2011).
39. J-S. Lyu et al., *Determination of the Interface Trap Density in Metal Oxide Semiconductor Field -Effect Transistor through Subthreshold Slope Measurement*. Jpn. J. Appl. Phys. **32**, 4393 (1993).
40. P. J. McWhorther and P. S. Winokur, *Simple Technique for Separating the Effects of Interface Traps and Trapped Oxide Charge in Metal-oxide-*semiconductor Transistors, Appl. Phys. Lett. **48**, 133 (1986).
41. G. Binning et al., Surface studied by scanning tunneling microscopy. Phys. Rev. Lett. **49**, 57 (1982).
42. G. Binning et al., Atomic force microscope. Phys. Rev. Lett. **56**, 930 (1982).

43. S. Morita, F.J. Giessibl, R. Wiesendanger, Noncontact atomic force microscopy. vol.**2**, Springer-Verlag, Heidelberg (2009).

44. F.J. Giessibl, Atomic resolution of silicon (111)-(7x7) surface by atomic force microscopy. Science **267**, 68 (1995).

45. M. Nonnenmacher et al., Kelvin probe force microscopy Appl. Phys. Lett. **58**, 2921 (1991).

46. L. Kelvin, Contact electricity of metals Phil. Mag. **46**, 82 (1898)

47. W. Melitz et al., Kelvin probe force microscopy and its application. Surf. Sci. Rep. **66**, 1-27 (2011).

48. S. Sadewasser, T. Glatzel, Kelvin Probe Force Microscopy – Measuring and compensating electrostatic forces. Springer-Verlag, Hedelberg (2012)

49. A.K. Henning and T.Hochwitz, Scanning probe microscopy for 2-D semiconductor dopant profiling and device failure analysis. Mat. Sci. Eng. B **42**, 88 (1996).

50. S. Sadewasser et al., High-resolution work function imaging of single grains of semiconductor surface. Appl. Phys. Lett. **80**, 2979 (2002).

51. L. Gross et al., Measuring the Charge State of an Adatom with Noncontact Atomic Force Microscopy. Science **324**, 1428 (2009).

52. S. Kitamura et al., Atomic-scale variations in contact potential difference on Au/Si(111) 7×7 surface in ultrahigh vacuum Appl. Surf. Sci. **157**,222 (2000)

53. G. H. Enevolsden et al., Atomic Scale Kelvin Probe Force Microscopy Studies of the Surface Potential Variations on the TiO2(110) Surface. Phys. Rev. Lett **100**, 236104 (2008)

54. S. Sadewasser et al., New Insights on Atomic-Resolution Frequency-Modulation Kelvin-Probe Force-Microscopy Imaging of Semiconductors Phys. Rev. Lett **103**, 266103 (2009)

55. M. Ligowski et al., Observation of individual dopants in a thin silicon layer by low temperature Kelvin Probe Force Microscope Appl. Phys. Lett. **93**, 142101 (2008).

56. M. Anwar et al., Single-Electron Charging in Phosphorus Donors in Silicon

Observed by Low-Temperature Kelvin Probe Force Microscope. Jpn. J. Appl. Phys. **50**, 08LB10 (2011).

57. M. Anwar et al., Effect of electron injection into phosphorus donors in silicon-on-insulator channel observed by Kelvin probe force microscopy Appl. Phys. Lett. **99**, 213101 (2011).
58. R. Nowak et al., Effects of deep-level dopants on the electronic potential of thin Si pn junctions observed by Kelvin probe force microscope Appl. Phys. Lett. **102**, 083109 (2013).
59. P.P. Altermatt et al., A simulation model for the density of states and for incomplete ionization in crystalline silicon. I. Establishing the model in Si: P. J. Appl. Phys. **100**, 113714 (2006).
60. G.A. Thomas et al., Optical study of interacting donors in semiconductors Phys. Rev. B. **23**, 5472 (1981)..
61. B. Weber et al., Ohm's Law Survives to the Atomic Scale, Science **335**, 64 (2012).
62. A. Tilke et al., *Coulomb blockade in quasimetallic silicon-on-insulator nanowires,* Appl. Phys. Lett. **75**, 3704 (1999).
63. J. A. Nixon and J. H. Davies, *Potential fluctuations in heterostructure device.* Phys. Rev. B **41**, 7929 (1990).
64. G. J. Evans, H. Mizuta, and H. Ahmed, *Modeling of structural and threshold voltage characteristics of randomly doped silicon nanowires in the Coulomb-blockade regime* Jpn. J. Appl. Phys. **40**, 5837 (2001).
65. J.H. Davies et al., *Realistic models of quantum devices*. IWCM p.61-66 (1992).
66. C. Kittel, *Introduction to Solid State Physics* (Wiley, 2005) 8th ed., p. 404.
67. T-W. Tang et al., *Thomas–Fermi approximation for a two-dimensional electron gas at low temperatures.* J. Appl. Phys, **95,** 7990 (2004).

Publications

Journal papers

Tyszka K, Moraru D, Mizuno T, Jablonski R, Tabe M (2015) Comparative study of donor-induced quantum dots in Si nano-channels by single-electron transport characterization and Kelvin probe force microscopy.
Journal of Applied Physics 117: 244307

Tyszka K, Moraru D, Mizuno T, Jablonski R, Tabe M (2015) Kelvin probe force microscope observation of donors' arrangement in Si transistor channel.
Advanced Materials Research 1117: 82-85

Tyszka K, Moraru D, Mizuno T, Jablonski R, Tabe M (2015) Effect of selective doping on the spatial dispersion of donor-induced quantum dots in Si nanoscale transistors.
Applied Physics Express 8: 094202 1-4

Proceedings and extended abstracts

Tyszka K, Moraru D, Mizuno T, Jablonski R, Tabe M (2014) KPFM Observation of Quantum Dots Induced by Clustered Donors in Selectively-Doped SOI-FETs. 46th International Conference on Solid State Device and Materials, Extended Abstracts: 798-799

Tyszka K, Moraru D, Mizuno T, Jablonski R, Tabe M (2015) Position and Number Control of Donor-QD Potential by Pattern-doping in SOI-FET Channels. IEEE Silicon Nanoelectronics Workshop, Workshop Abstracts: p.39

Tyszka K, Moraru D, Mizuno T, Jablonski R, Tabe M (2014) KPFM observation of donors in field effect transistor channel. 16th Takayanagi Kenjiro Memorial Symposium - Toward Advanced Imaging Science Creation, Proceedings: PS1-9- 1–3

Tyszka K, Nowak R, Moraru D, Mizuno T, Jablonski R, Tabe M (2013) Surface potential measurement of selectively-doped FETs by KPFM. 15th Takayanagi Kenjiro Memorial Symposium - Toward Advanced Imaging Science Creation, Proceedings: S4-13- 1-5

Moraru D, **Tyszka K**, Samanta A, Takasu Y, Tsutaya T, Mizuno T, Jablonski R, Tabe M (2014) Silicon Nanoscale Transistors with Dopant-Induced Quantum Dots. 2nd International Conference on Nano Electronics Research and Education, Proceedings: 55-56

Moraru D, **Tyszka K**, Samanta A, Takasu Y, Tsutaya T, Mizuno T, Jablonski R, Tabe (2015) Impact of diffused donor-clusters near lead/channel boundary on high-temperature single-electron tunneling in narrow SOI-FETs. IEEE Silicon Nanoelectronics Workshop, Workshop Abstracts: p.31

Tan N.H, Moraru D, **Tyszka K**, Sapteka A, Puriwyanti S, Anh L.T, Manoharan M, Mizuno T, Jablonski R, Hartanto D, Mizuta H, Tabe M (2015) Dopant-assisted tunnel-current enhancement in two-dimensional Esaki diodes. IEEE Silicon Nanoelectronics Workshop, Workshop Abstracts: p.95

Samanta A, Moraru D, Kuzuya Y, **Tyszka K**, Anh L. T, Mizuno T, Jablonski R, Mizuta H,Tabe M (2013) Dopant-Atom-based SOI-Transistors by Selective Nanoscale Doping. 45th International Conference on Solid State Device and Materials, Extended abstract: 788-789

Conference presentations

Tyszka K, Moraru D, Mizuno T, Jablonski R, Tabe M (2015) Position and Number Control of Donor-QD Potential by Pattern-doping in SOI-FET Channels. The 2015 Silicon Nanoelectronics Workshop, Kyoto, Japan

Tyszka K, Moraru D, Mizuno T, Jablonski R, Tabe M (2014) KPFM Observation of Quantum Dots Induced by Clustered Donors in Selectively-Doped SOI-FETs. 46th International Conference on Solid State Device and Materials Tsukuba, Japan

Tyszka K, Moraru D, Mizuno T, Jablonski R, Tabe M (2015) Surface potential observation of heavily-doped Si by KPFM. 62th JSAP Spring Meeting, Kanagawa, Japan

Tyszka K, Moraru D, Mizuno T, Jablonski R, Tabe M (2014) KPFM Imaging of Donor Clusters in Selectively-Doped SOI-FET. 75th JSAP Autumn Meeting, Sapporo, Japan

Tyszka K, Moraru D, Mizuno T, Jablonski R, Tabe M (2013) KFM Measurement of Nano-Scale Selectively Doped Silicon Channel. 74th JSAP Autumn Meeting, Doshisha, Kyoto, Japan

Tyszka K, Moraru D, Mizuno T, Jablonski R, Tabe M (2014) Kelvin Probe Force Microscope observation of donors' arrangement in Si transistor channel. 13th International Conference on Global Research and Education, Inter-Academia 2014, Riga, Latvia

Tyszka K, Moraru D, Mizuno T, Jablonski R, Tabe M (2014) KPFM observation of

donors in field effect transistor channel. 16th Takayanagi Kenjiro Memorial Symposium - Toward Advanced Imaging Science Creation. Hamamatsu, Japan

Tyszka K, Nowak R, Moraru D, Mizuno T, Jablonski R, Tabe M (2013) Surface potential measurement of selectively-doped FETs by KPFM. 15th Takayanagi Kenjiro Memorial Symposium - Toward Advanced Imaging Science Creation, Hamamatsu, Japan

Tyszka K, Moraru D, Mizuno T, Jablonski R, Tabe M (2015) KPFM observation of donors in transistor channels doped with different concentrations. International Symposium Towards the Future of Advanced Researches, Hamamatsu, Japan

Others

Moraru D, **Tyszka K**, Takasu Y, Samanta A, Mizuno T, Jablonski R, Tabe M (2015) Physics of strongly-coupled dopant atoms in nanodevices. IEEE International Conference on Quality in Research, Lombok, Indonesia

Moraru D, **Tyszka K**, Samanta A, Takasu Y, Tsutaya T, Mizuno T, Jablonski R, Tabe (2015) Impact of diffused donor-clusters near lead/channel boundary on high-temperature single-electron tunneling in narrow SOI-FETs. IEEE Silicon Nanoelectronics Workshop, Kyoto, Japan

Moraru D, **Tyszka K**, Samanta A, Mizuno T, Jablonski R, Tabe M (2015) Tunneling Transport via Dopant-induced Quantum Dots in Silicon Nano-devices. International Conference on Nanoscience and Nanotechnology, Tamil Nadu, India

Moraru D, **Tyszka K**, Samanta A, Takasu Y, Tsutaya T, Mizuno T, Jablonski R, Tabe M (2014) Silicon Nanoscale Transistors with Dopant-Induced Quantum Dots. 2nd International Conference on Nano Electronics Research and Education, Hamamatsu, Japan

Tan N.H, Moraru D, **Tyszka K**, Sapteka A, Puriwyanti S, Anh L.T, Manoharan M, Mizuno T, Jablonski R, Hartanto D, Mizuta H, Tabe M (2015) Dopant-assisted tunnel-current enhancement in two-dimensional Esaki diodes. IEEE Silicon Nanoelectronics Workshop, Kyoto, Japan

Moraru D, Samanta A, **Tyszka K**, Mizuno T, Jablonski R, Tabe M (2015) Tunneling via Single and Coupled Dopant Atoms in Si Nanodevices. Energy Materials Nanotechnology Meeting on Quantum Technology, Beijing, China

Tabe M, Nowak R, **Tyszka K**, Moraru D, Mizuno T, Jablonski R (2013) Detection of

dopant potential in silicon nano-channel by low-temperature. 12th International Conference on Global Research and Education, Inter-Academia, Sofia, Bulgaria

Tabe M, Moraru D, Samanta A, **Tyszka K**, Tan H.N, Takasu Y, Jablonski R (2015) Effect of individual dopants in nano-SOI-MOSFETs and nano-pn-diodes. ECS ULSI Process Integration 9 Conference, Phoenix, USA

Samanta A, Moraru D, Kuzuya Y, **Tyszka K**, Anh L. T, Mizuno T, Jablonski R, Mizuta H,Tabe M (2013) Dopant-Atom-based SOI-Transistors by Selective Nanoscale Doping. 45th International Conference on Solid State Device and Materials, Fukuoka, Japan